



OPEN ACCESS

EDITED BY

Hossein Azizi,
University of Kurdistan, Iran

REVIEWED BY

Takeshi Kuritani,
Hokkaido University, Japan
Abdolnaser Fazlnia,
Urmia University, Iran
Ali Reza Davoudian,
Shahrekord University, Iran
Kwan-Nang Pang,
Academia Sinica, Taiwan

*CORRESPONDENCE

Olaya Dorado,
✉ odorado@geo3bcn.csic.es

SPECIALTY SECTION

This article was submitted to
Petrology, a section of the journal
Frontiers in Earth Science

RECEIVED 31 January 2023

ACCEPTED 13 March 2023

PUBLISHED 28 March 2023

CITATION

Dorado O, Wolff JA, Ramos FC and
Martí J (2023), Ba, Sr, and Rb feldspar/
melt partitioning in recent eruptions from
Teide-Pico Viejo volcanic complex,
Tenerife: New insights into pre-
eruptive processes.
Front. Earth Sci. 11:1155724.
doi: 10.3389/feart.2023.1155724

COPYRIGHT

© 2023 Dorado, Wolff, Ramos and Martí.
This is an open-access article distributed
under the terms of the [Creative
Commons Attribution License \(CC BY\)](#).
The use, distribution or reproduction in
other forums is permitted, provided the
original author(s) and the copyright
owner(s) are credited and that the original
publication in this journal is cited, in
accordance with accepted academic
practice. No use, distribution or
reproduction is permitted which does not
comply with these terms.

Ba, Sr, and Rb feldspar/melt partitioning in recent eruptions from Teide-Pico Viejo volcanic complex, Tenerife: New insights into pre-eruptive processes

Olaya Dorado^{1,2*}, John A. Wolff³, Frank C. Ramos⁴ and
Joan Martí¹

¹Geosciences Barcelona, Consejo Superior de Investigaciones Científicas, Barcelona, Spain,

²Departament de Mineralogia, Petrologia i Geologia Aplicada, Facultat de Ciències de la Terra, Universitat de Barcelona, Barcelona, Spain, ³School of the Environment, Washington State University, Pullman, WA, United States, ⁴Department of Geological Sciences, New Mexico State University, Las Cruces, NM, United States

The behaviour of Group I and II elements during the petrogenesis of felsic igneous rocks is largely controlled by feldspar-liquid relationships. Numerous experimental studies have addressed plagioclase/melt element partitioning, with fewer studies devoted to potassium feldspar, and very few to albite-rich ternary-composition feldspar (An ~ Or < Ab). However, the partition coefficient for Ba is known to increase by at least an order of magnitude through the crystallisation sequence sodic plagioclase–anorthoclase–potassium feldspar that is typical of sodic alkaline suites. Feldspars, glasses, and whole rocks in such suites may exhibit strong enrichments and depletions that can be used to track processes of crystal fractionation, cumulate formation, and cumulate recycling. Here, we review experimental feldspar/melt partitioning data for Ba, Sr, and Rb for all feldspars. Regression of available data provides expressions that appear to adequately model the compositional and temperature dependence of partition coefficients for albite-rich compositions. We have applied this model to feldspar and melt compositions of the products of several Holocene eruptions (Pico Viejo C, Pico Viejo H, Teide J2, Lavas Negras, Arenas Blancas, Montaña Rajada and Montaña Reventada) of the basanitic-phonolitic suite of the Teide-Pico Viejo volcanic system (Tenerife, Spain), using EPMA and LA-ICP-MS analyses. Comparing analysed feldspar/groundmass pairs with predicted partition coefficients obtained with the models provides a way of distinguishing between feldspars that are in or out of equilibrium with their host melt, and of reconstructing feldspar histories. The results demonstrate the existence of a distinct population of feldspars that had undergone accumulation, fusion and recrystallisation events, in Lavas Negras and Arenas Blancas flows. In addition, the anomalous trachytic composition of Montaña Reventada is due to melting of a feldspar-dominated cumulate. Application of these techniques to active magmatic systems will allow us a better understanding of different pre-eruptive processes, and ultimately improve volcanic hazard assessment.

KEYWORDS

crystal mush, cumulate melting, alkaline magmatism, reservoir dynamics, multiple regression analysis, partition coefficients, trace elements, barium enrichments

1 Introduction

Petrological investigations of past eruptions provide a means of monitoring the evolution of magmatic systems that feed active volcanoes. It is now well understood that such systems may be structurally, petrologically, and dynamically complex, especially at long-lived volcanic centers with diverse eruption styles and magma types. Explosive felsic magmas are thought to develop in the shallow parts of deep-rooted, trans-crustal magma systems (e.g., Sparks et al., 2019). Detailed relationships between crystals and their enclosing melt phase in volcanic rocks provide one avenue to understanding Earth evolution and the dynamics of volcanic feeding systems (Blundy and Wood, 2003; Ramos and Tepley, 2008). Moreover, they are necessary for accurate calculation of magmatic timescales using diffusion chronometry (e.g., Costa et al., 2003), and for dating of single crystals (Ramos et al., 2019; Brown et al., 2022).

The respective interpretation of whole rock geochemistry of volcanic rocks and micro-analyses of their mineral assemblages, textures, and compositional variations within the crystals is key to deciphering processes occurring within a magmatic system (e.g., crystallisation and melting processes, magma mixing, recharge events, contamination with the host rock, eruption triggering, accumulation of crystals, etc.). Understanding these processes is of great importance as it allows the identification of events that may be repeated in current active magmatic systems and assists preparation for the eruptions to come. These concepts have largely been developed in the context of relatively silica-rich, metaluminous rocks (andesites, dacites and rhyolites) erupted in association with active continental margins (e.g., Browne et al., 2006; Salisbury et al., 2008; Kent et al., 2010). Alkaline felsic volcanoes erupting trachytes and phonolites show many similarities to their metaluminous counterparts, but exhibit important differences in chemistry, mineralogy, and phase relations that present distinct challenges and opportunities for understanding their parent subsurface systems.

Especially in the case of active volcanoes with short intervals between successive eruptions, magma plumbing systems are likely to contain a variety of magma bodies. These bodies may be characterised by a wide range of crystallinities, although highly ($\geq 50\%$) crystalline, and therefore static, mush may be the most common form of stored magma (Bachmann and Bergantz, 2008; Huber et al., 2009; Huber et al., 2012). High-crystallinity mushes, including essentially solid rocks with interstitial melt (cf. “rigid sponge” of Hildreth, 2004) are easily remobilised by new rising magma, due to the reduced thermal penalty compared to that required to recycle solid country rock. Therefore, phenocrysts in volcanic rocks may have grown from the enclosing magma or may be entrained from or introduced (antecrysts and xenocrysts) *via* other magma, mush, or solid rocks with which the carrier magma interacted prior to eruption. The plethora of such potentially contributing materials may lead to highly complex crystal origins in any one parcel of erupted magma. Unravelling the complex relations between these different materials to gain insight into magma dynamics requires a detailed study of crystal populations and crystal-melt relations.

Feldspar is the dominant mineral phase in felsic igneous rocks. Therefore, knowledge of feldspar/melt partition coefficients is

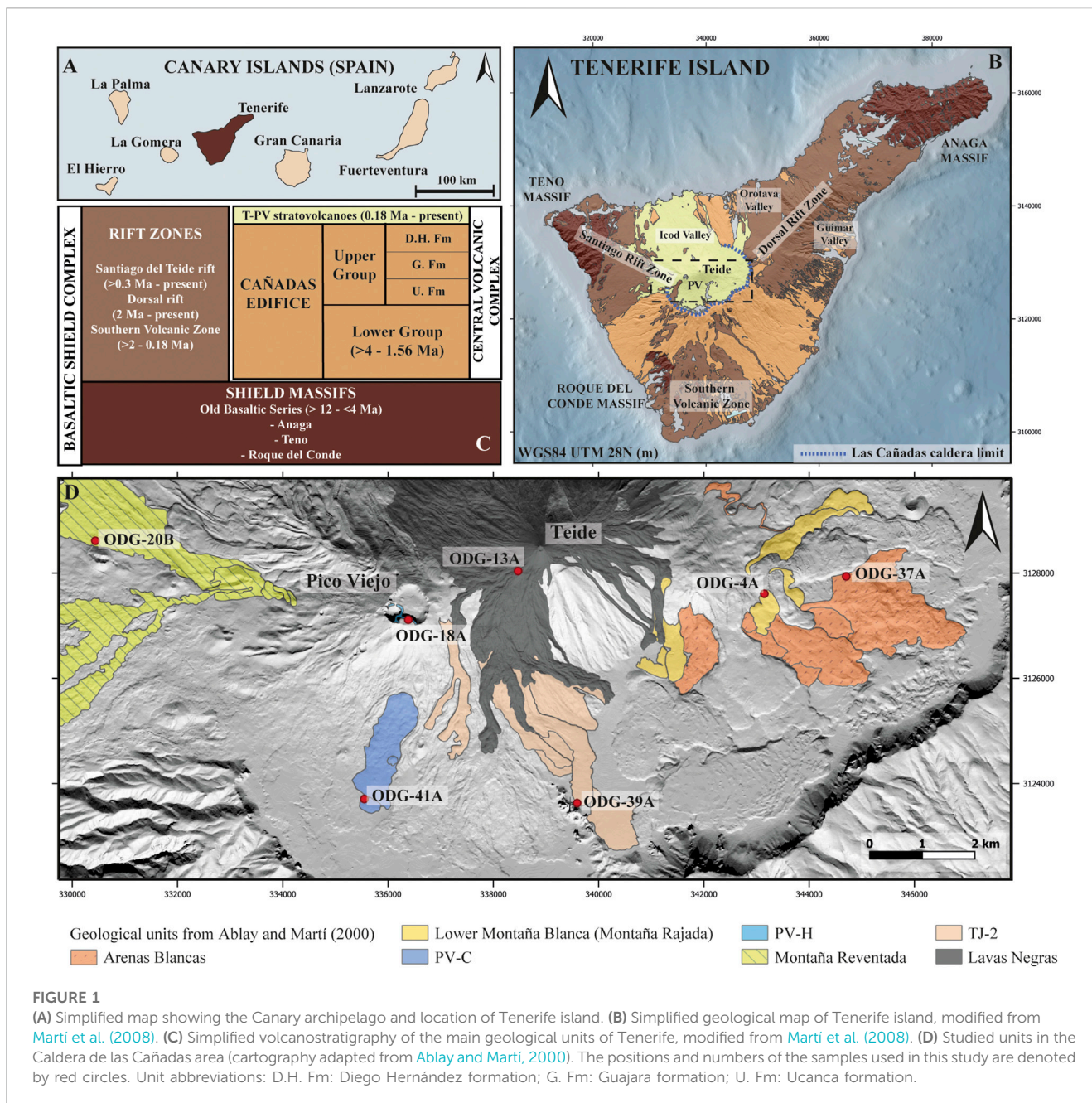
critical in unravelling the potentially complex history of felsic volcanic rocks. Many alkaline suites, especially of sodic affinity, have anorthoclase as the dominant feldspar. Although there are numerous experimental studies of plagioclase/melt element partitioning, fewer data are available for alkali feldspar, and very few for anorthoclase (compilation of Wolff et al., 2020). Our goals in this paper are twofold: 1) to derive working values of trace element partition coefficients, especially for the anorthoclase compositional range, for Rb, Sr, and Ba, trace elements sensitive to feldspar crystallisation or melting; 2) to apply these to modeling magmatic evolution of historic and Holocene phonolites and associated rocks from Teide volcano in the Canary Islands.

2 Geological setting

Tenerife is the largest island in the Canary archipelago, located in the east-central Atlantic Ocean off the west coast of Africa. Tenerife rises almost 8 km from the underlying oceanic crust (Watts et al., 1997), making it one of the largest volcanic islands in the world. The oldest dated subaerial rocks on Tenerife (an 11.6 Ma basaltic dike, Ancochea et al., 1990) indicate that the island began to grow prior to 12 Ma. The formation of the island began as a shield volcano complex that now composes almost 90% of the total volume of the island. This shield complex, the Old Basaltic Series, consists mainly of alkali basalts and basanites, which are now exposed in the three corners of the island, in the massifs of Teno, Anaga, and Roque del Conde (Figure 1). This first stage of volcanism lasted until 3.8 Ma (Fuster et al., 1968; Ancochea et al., 1990; Thirlwall et al., 2000; Guillou et al., 2004). Basaltic eruptions have continued during repose periods between phonolitic eruptions in the central part of the island, and during historical times along the two rift zones (Santiago del Teide and Dorsal ridges) and in the Southern Volcanic Zone as monogenetic volcanic fields (Cas et al., 2022).

A basanitic-phonolitic volcanic construct, the Las Cañadas edifice, began to develop in the central part of the island at ~ 3.8 Ma (Fuster et al., 1968; Araña, 1971; Ancochea et al., 1990; Martí et al., 1994). Rocks associated with the Las Cañadas edifice are divided into a Lower Group and an Upper Group. The Lower Group (3.8–2.2 Ma) consists of lavas and pyroclastic rocks of mafic, intermediate, and phonolitic compositions. The Upper Group (1.57–0.19 Ma) includes three distinct basanite to phonolite cycles, characterised by highly explosive phonolitic activity, represented by the Ucanca, Guajara, and Diego Hernández Formations (Martí et al., 1994), each culminating in a major caldera-forming eruption: the Ucanca cycle at 1.02 Ma, Guajara at 0.57 Ma; and Diego Hernández at 0.19 Ma (Martí et al., 1994; Martí et al., 1997; Martí and Gudmundsson, 2000; Carracedo et al., 2007; Edgar et al., 2007; Cas et al., 2022). These processes gave shape to the Las Cañadas caldera (LCC), a depression formed from the three individual overlapping calderas. In addition, massive landslides, occasionally linked to some of these caldera-forming eruptions, formed the Guimar, La Orotava, and Icod valleys (Martí et al., 1997; Hunt et al., 2018; Cas et al., 2022).

A fourth cycle, currently active, is represented by the Teide-Pico Viejo (T-PV) volcanic complex within the Las Cañadas caldera. This complex consists of the twin stratovolcanoes, Teide and Pico Viejo, and several flank vents. The composite cones of Teide and Pico Viejo started to develop at about 170–190 ka (Martí et al., 1994; Brown



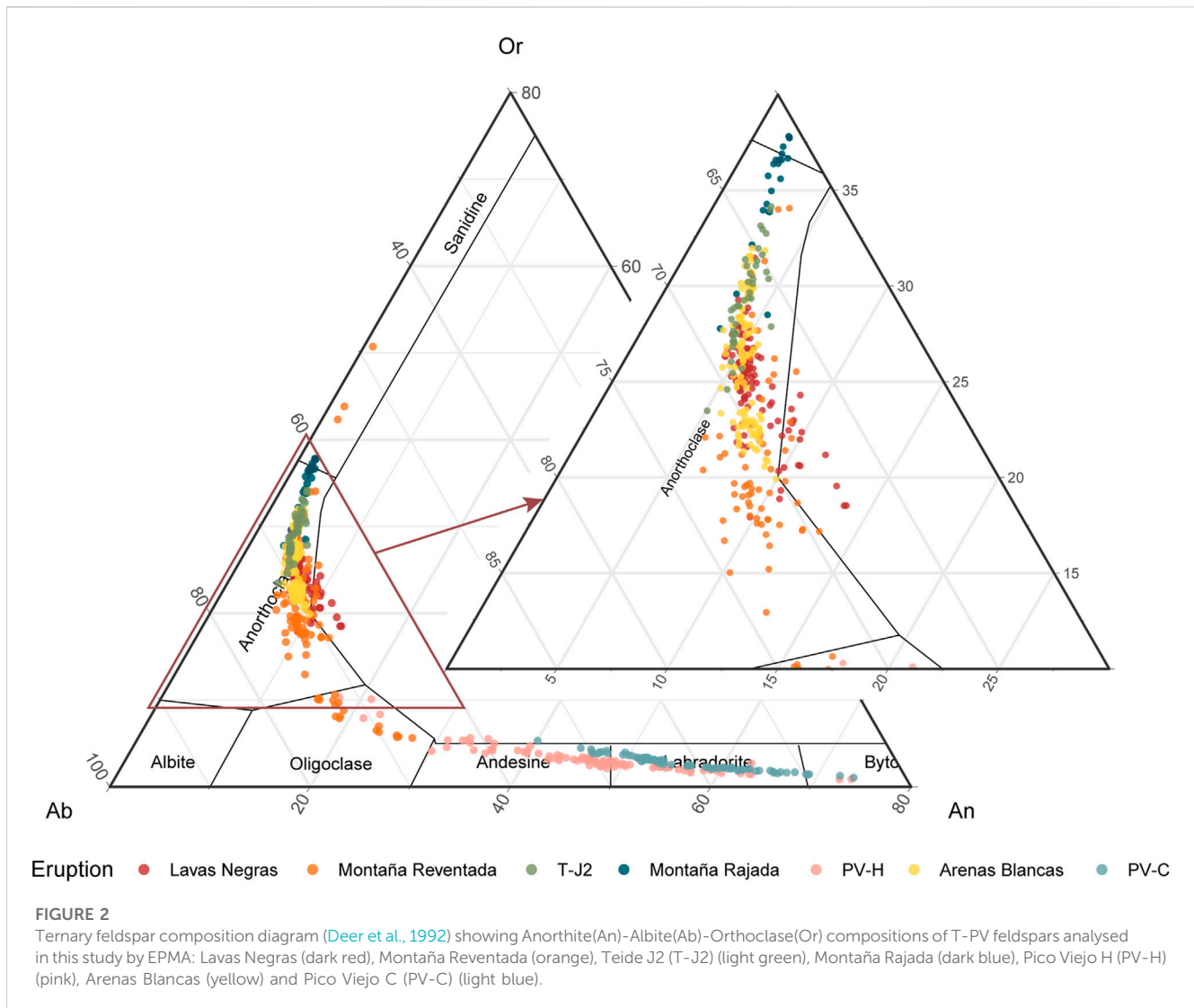
et al., 2003; Edgar et al., 2007; Guillou et al., 2013). The first stages of construction of T-PV were dominated by mafic to intermediate magmas. Phonolites began to appear at ~35 ka and have become the dominant erupted composition since (Ablay et al., 1998; Ablay and Martí, 2000; Martí et al., 2008). Phonolite eruptions on the flanks of these cones have been the most explosive (Ablay et al., 1995; Martí et al., 2008; García et al., 2012).

Petrological data suggest that interaction between a deep basaltic magma reservoir and a shallow phonolitic magmatic system has dominated the evolution of the T-PV complex. In fact, most phonolite units show evidence of magma mixing, and their eruptions were likely triggered by the intrusion of hotter magmas originating from deeper levels (Araña et al., 1994; Triebold et al., 2006; Wiesmaier et al., 2011; Albert et al., 2015b; Dorado et al., 2021).

3 Materials and methods

3.1 Multiple regression analysis of experimental partitioning data

We seek a working description of the variation in feldspar/melt partition coefficients for the elements Rb, Sr, and Ba for all feldspars, with particular attention to ternary compositions (Ab >> An ~ Or). Most natural sodic plagioclase has significant K, and most natural anorthoclase has significant Ca, including those of interest here (Figure 2). Although there is a large amount of data from natural samples (e.g., Bédard, 2006), we have elected to use only experimental data. For multiple regression analyses, we used experimental data reported in 11 studies that crystallised feldspar



compositions ranging from anorthite to sanidine using either natural or synthetic starting materials (Table 1). Data from 145 partition experiments were collected and, to avoid large errors arising from analyte concentrations close to detection limits, analyses reporting <0.5 ppm in glass or feldspar were rejected, leaving a residue of feldspar/melt values for Ba ($n = 145$), for Sr ($n = 141$) and for Rb ($n = 90$). Multiple linear regressions were calculated with the IMB SPSS Statistics (Version 25.0) software using R^2 of the model and the p -value of each individual variable to test the quality of the regressions and the significance of the different parameters used.

3.2 Samples and analytical methods

Natural samples used in this study were collected in Tenerife during a field campaign in March 2020. They have been registered in the online System for Earth Science Registration database (<http://www.geosamples.org>), where all the information related to the samples can be accessed (UTM coordinates, geological units

following the units described by Ablay and Martí, 2000). Four are phonolites: ODG-4A, 10.58052/IEODG000B (Montaña Rajada, 2–4 ka; Ablay et al., 1995; Brown et al., 2022); ODG-13A, 10.58052/IEODG000K (Teide L or Lavas Negras, 1.0 ka; Brown et al., 2022), ODG-37A, 10.58052/IEODG001B (Arenas Blancas, 4 ka; Brown et al., 2022) and ODG-39A, 10.58052/IEODG001D (Teide J2, between 2 and 2.6 ka; Carracedo et al., 2003; Carracedo et al., 2007; Martí et al., 2008). Two are phonotephrites: ODG-18A, 10.58052/IEODG000P (PV-H, <15 ka; Carracedo et al., 2003; Carracedo et al., 2007; Martí et al., 2008) and ODG-41A, 10.58052/IEODG001F (PV-C, >18 ka; Carracedo et al., 2003; Carracedo et al., 2007; Martí et al., 2008). One trachyte from the 0.9–1.1 ka (Carracedo et al., 2007; Risica et al., 2020) Montaña Reventada eruption (ODG-20B, 10.58052/IEODG000S) is also included. This trachyte shows signatures of magma mixing both in field and thin section observations. Locations of these samples are shown in Figure 1.

Whole rock analyses (major, minor, and trace elements) were performed at the Peter Hooper GeoAnalytical Lab at Washington State University, using X-ray fluorescence (XRF) and inductively

TABLE 1 Summary of experimental studies on the plagioclase-feldspar/melt element partitioning used in the multiple regression analysis in this study. ^aAlkali feldspar, ^bplagioclase. Mineral abbreviations after [Whitney and Evans \(2010\)](#).

References	Feldspar composition	Starting material	Experimental conditions	Analytical methods	N° data
Long (1978)	Afsp ^a	Synthetic granite gel (An ₇ Ab ₂₅ Or ₄₀ Q ₂₄) + trace elements	720°C–780°C, 8 kb	EPMA	32
Icenhower and London (1996)	Plag ^b + Afsp ^a	Synthetic metapelite composition (Qtz+Ab+Ms+Bt)	650°C–750°C, 2 kb	EPMA	12
Bindeman et al. (1998)	Plag ^b	Basaltic andesite + synthetic Ab and An	1,152.85°C–1,296.85°C, 0.001 kb	EPMA and SHRIMP	11
Bindeman and Davis (2000)	Plag ^b	Basaltic andesite + synthetic Ab and An. REE-doped	1,152.85°C–1,296.85°C, 0.001 kb	EPMA and SHRIMP	12
Aigner-Torres et al. (2007)	Plag ^b	Basalt (MORB)	1,180°C–1,220°C, 0.01 kb	EPMA and LA-ICP-MS	10
Fabrizio et al. (2009)	Plag ^b + Afsp ^a	Synthetic mixture of reagent oxides, silicates and CaCO ₃ + Ra	750°C–1,410°C, 0.001–10 kb	EPMA and LA-ICP-MS	6
Tepley et al. (2010)	Plag ^b	Natural and synthetic basaltic and basaltic andesite	1,127°C–1,265°C, 0.001 kb	EPMA, SIMS and LA-ICP-MS	6
Henderson and Pierozynski (2012)	Afsp ^a	Synthetic metaluminous compositions with and without An added and peralkaline compositions without Ca	850°C–905°C, 1 kb	EPMA	8
Dohmen and Blundy (2014)	Plag ^b	Mixtures of Di + An + Ab gels + trace elements	1,086°C–1,290°C, 0.01 kb	EPMA and SIMS	17
Arzilli et al. (2018)	Afsp ^a	Trachytic melt (Breccia Museo Member, Campanian Ignimbrite)	870°C–890°C, 5 kb	EPMA and LA-ICP-MS	2
Schoneveld and O'Neill (2019)	Plag ^b	Silicate melts from the CAS and CMAS system	1,332°C–1,453°C, 0.01–10 kb	EPMA and LA-ICP-MS	29

coupled plasma mass spectrometry (ICP-MS). Complete details about the equipment, methods, and procedures are described at <https://environment.wsu.edu/facilities/geoanalytical-lab/technical-notes/>.

Feldspar and glass samples were also analysed for major and trace elements using a JEOL JXA8500F field emission electron microprobe in the same laboratory. All analyses were performed using a 15 kV accelerating voltage, a 15 nA current, and a beam diameter of 5 µm. Data were acquired and reduced with Probe For EPMA (PFE). Mean Atomic Number background estimates were used for all elements, except Al and Si, which were acquired using EDS, and processed through PFE with full standardization and matrix corrections. Negative values and values below detection of each element are reported as zero. Although an exhaustive study of mineral zoning from cores to rims of the minerals has been performed, only the analyses of the outer rims are used in calculating apparent partition coefficients here.

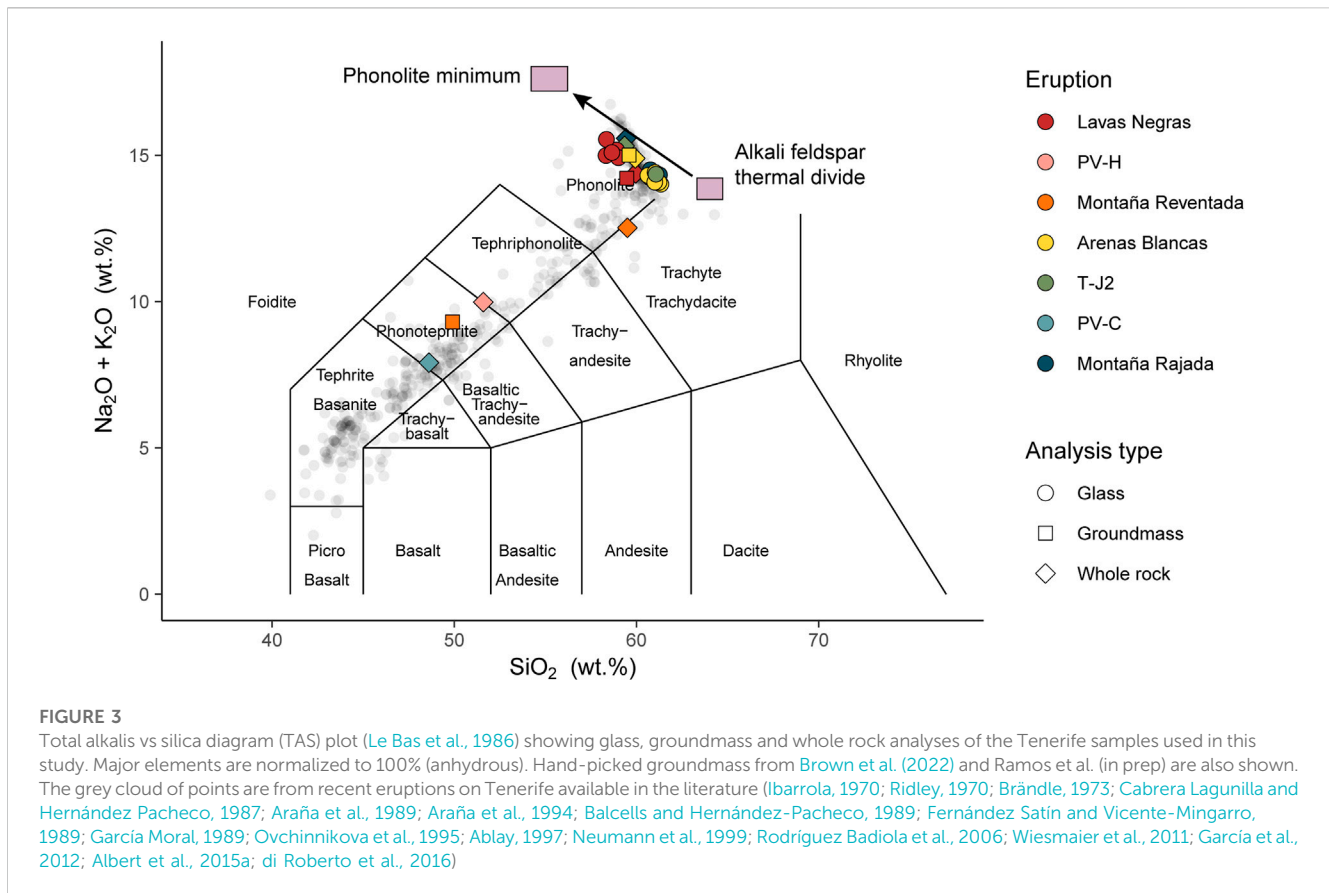
Selected minerals and glasses were also analysed for trace elements using laser ablation inductively coupled mass spectrometry (LA-ICP-MS). Analyses were performed in the same laboratory using an Agilent 7700 Series ICP-MS combined with a New Wave UP-213 laser ablation system. A spot size of 30 µm was used with a ~10.6 J/cm³ beam energy at 20 Hz. Analyses were collected along transects parallel to crystal faces to minimize potential mixing between chemical zones. Laser track lengths varied according to the available glass and feldspar sizes (from 100 µm to 500 µm). Data was normalized to NIST 610 standard using ²⁹Si as an internal reference. BCR-2 was used as an external standard.

Chemical data from this work are available in the [Supplementary Material](#). It should be noted that different ranges in concentrations for Sr and Ba were determined by EPMA and LA-ICPMS in feldspars from most samples. The discrepancy arises due to differences in the spatial resolution of the two techniques. The smaller electron beam was preferentially used on very fine zones and melt inclusion-rich areas where a clean analysis couldn't be obtained with the much wider laser beam. Laser ablation analysis focused on obtaining accurate and precise values for Sr and Ba at crystal edges, to facilitate the calculation of apparent partition coefficients. Rubidium concentrations are below EPMA detection limits, so all microanalytical Rb data reported here are from LA-ICP-MS.

4 Results

4.1 Multiple linear regression analyses

Enter, Forward, and Backward Stepwise methods were employed in the regression analyses to find the expression that best fits the experimental data using the fewest number of significant independent variables. In the Enter method, all the independent variables are manually included in the regression analysis, while the stepwise method (forward or backward) automatically selects the best predictor variables. The Forward Stepwise method starts the model with zero variables and adds the most significant variable at each step until the best model is reached. The Backward Stepwise method starts by considering



all possible variables and removes the least significant variable at each step until the best fit is achieved.

Equations were calculated with $RT\ln D_{Ba}$, $RT\ln D_{Sr}$, and $RT\ln D_{Rb}$ (where R , T and D_i are the gas constant, $8.314 \text{ JK}^{-1}\text{mol}^{-1}$, the crystallisation temperature and the partition coefficient, respectively) treated as variables that were dependent on feldspar major element compositions expressed as Or , Ab , and An [calculated as $100 \cdot K / (K + Na + Ca)$, $100 \cdot Na / (K + Na + Ca)$ and $100 \cdot Ca / (K + Na + Ca)$, where K , Na , and Ca are atomic abundances]. We recognise that the derived values aren't truly independent of T , because different experimental studies employed different temperature ranges dictated by different melting ranges of liquids that crystallise feldspars ranging from calcic plagioclase to potassium feldspar (Table 1). Nonetheless, temperature ranges approximate those of natural melts that bear feldspars of similar composition, and we consider this approach to be sufficient for a working description. Melt structure parameters such as $Al / (Na + K + Ca)$ resulted in little improvement in quality when incorporated in the regressions, hence these were omitted; they have little influence on partitioning behaviour for these elements (Blundy and Wood, 1991; Blundy and Wood, 1994). The output of each regression is given as the intercept and the coefficient for the statistically significant independent variable for each element. Equations for the prediction of $RT\ln D_i$ (kJ mol^{-1}) that show the best fits are:

$$RT\ln D_{Ba} = 11.643 + 0.653 \cdot Or - 0.406 \cdot An - 0.007 \cdot Or^2 \quad (1)$$

$$RT\ln D_{Sr} = 21.277 + 0.460 \cdot Or - 0.164 \cdot An - 0.008 \cdot Or^2 - 0.001 \cdot An^2 \quad (2)$$

$$RT\ln D_{Rb} = -35.655 + 0.801 \cdot Or - 0.188 \cdot An - 0.005 \cdot Or^2 \quad (3)$$

All three equations present a good fit to the experimental data, with $R^2 = 0.959$ for Ba , $R^2 = 0.902$ for Sr , and $R^2 = 0.963$ for Rb . Standard errors calculated for the predicted values are ± 4.216 for $RT\ln D_{Ba}$, ± 2.498 for $RT\ln D_{Sr}$ and ± 4.670 for $RT\ln D_{Rb}$.

Knowing the temperature at which a natural feldspar crystallised (from thermometry or other information), these equations enable the D_{Ba} , D_{Sr} , and D_{Rb} of natural samples to be predicted, based only on feldspar major element composition.

4.2 Petrography of natural samples

The least evolved samples studied in this work (Figure 3) in this work are from two different lava flows from Pico Viejo volcano: PV-C (mafic phonotephrite) and PV-H (mafic tephriphonolite). PV-C is less evolved, and older as inferred by stratigraphic criteria (PV-C is >18 and PV-H is <15 ka; Carracedo et al., 2003; Carracedo et al., 2007; Martí et al., 2008). This unit consists of a pahoehoe lava flow that shows a porphyritic texture with plagioclase as the main phenocryst. In addition to plagioclase (24%), the mineral assemblage includes clinopyroxene (2.5%), olivine (1.5%), and Fe-Ti oxides (0.5%) in a dark vitric groundmass (66.5%) with

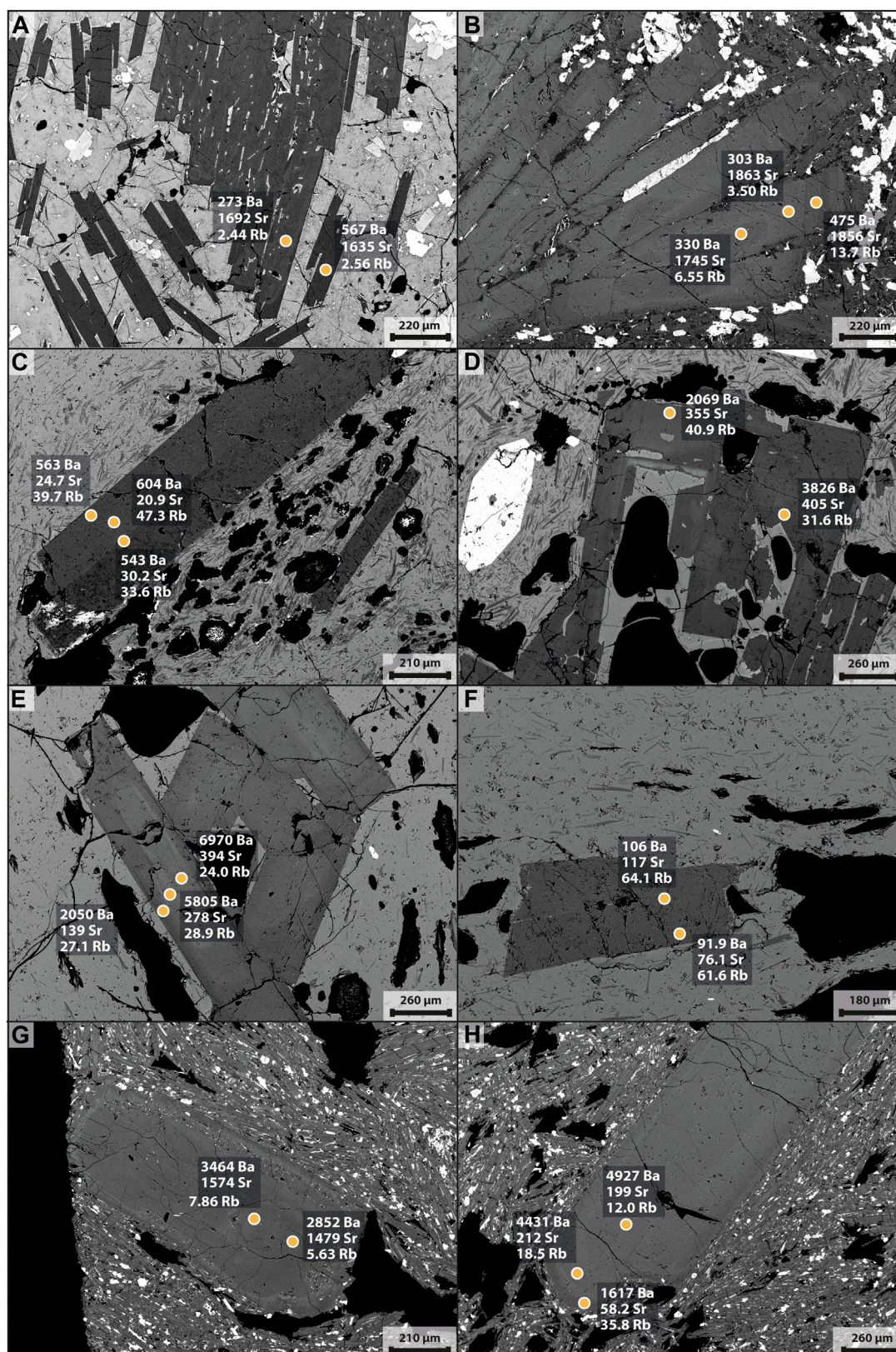
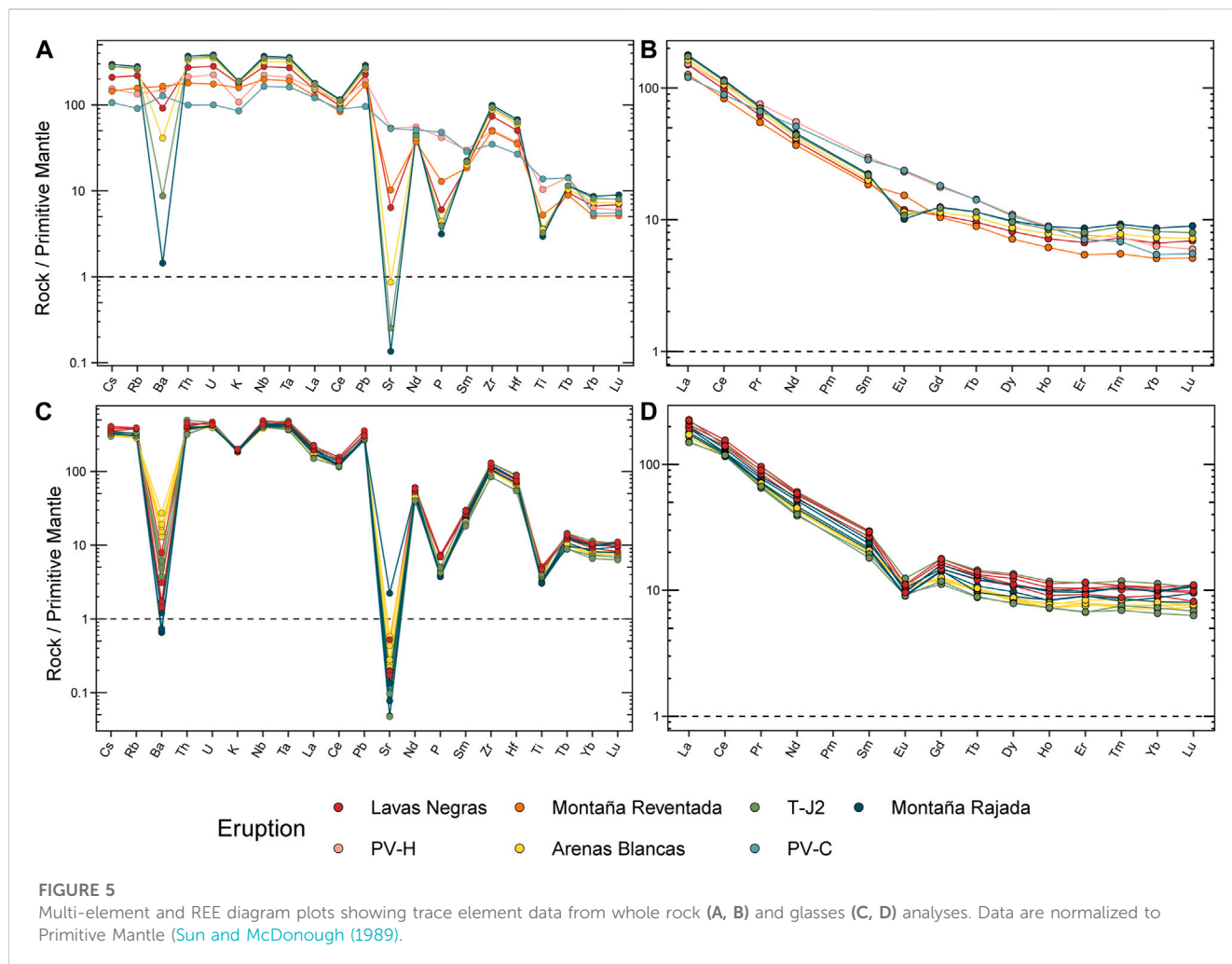


FIGURE 4

Back-scattered electron images showing representative feldspars from Tenerife samples. Yellow circles represent spots analysed using LA-ICP-MS. Values for Ba, Sr, and Rb are also given next to the appropriate analysis point. (A) PV-C (B) PV-H (C) T-J2 (D) Lavas Negras (E) Arenas Blancas (F) Montaña Rajada (G, H) Montaña Reventada.



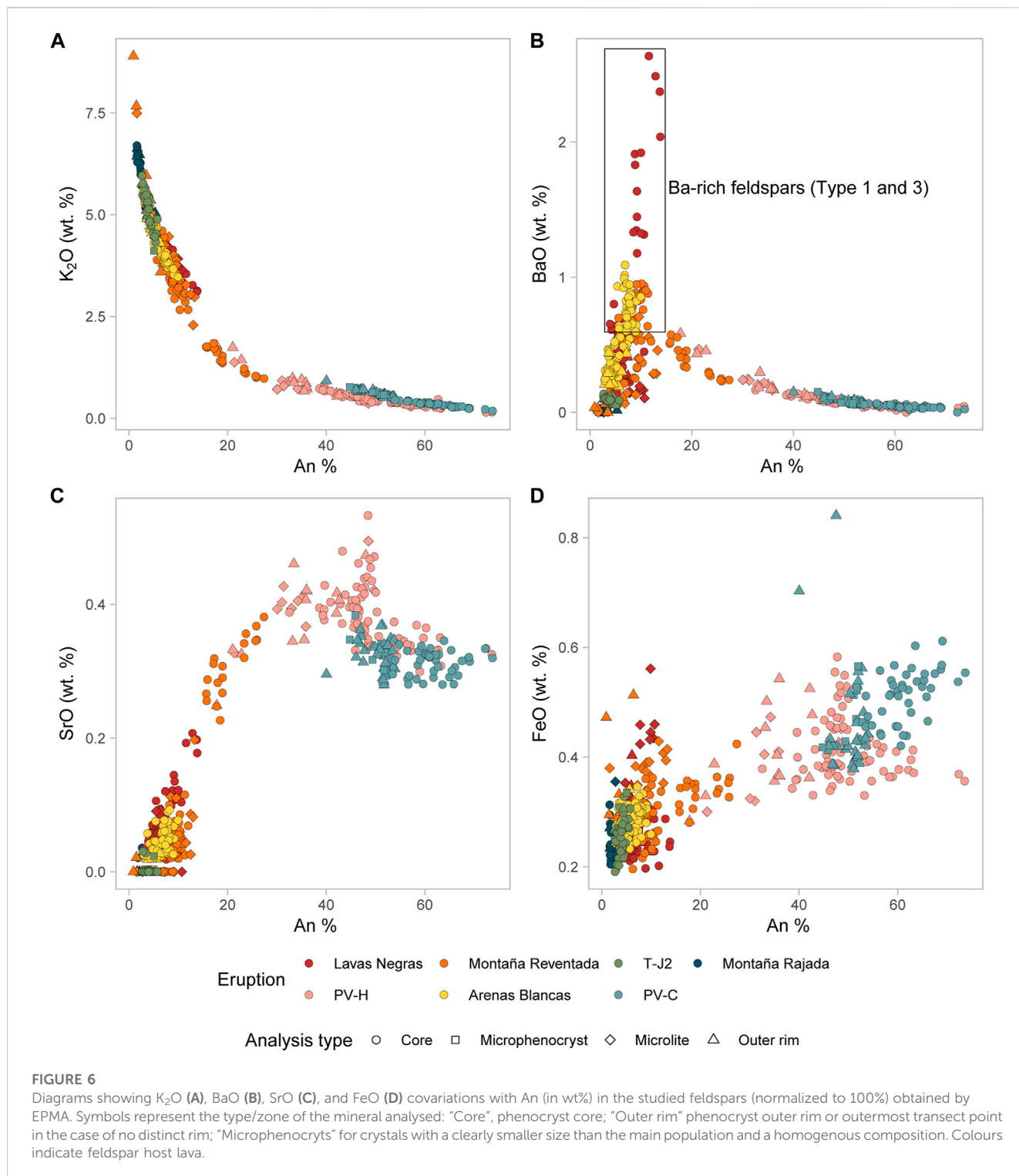
small microlites of plagioclase, Fe-Ti oxides, clinopyroxene and olivine, and 5% vesicles. Plagioclase phenocrysts in PV-C have spongy/cellular cores with inclusions of clinopyroxene, olivine and, mainly, glass (Figure 4A) with rounded edges and wide, euhedral rims. In addition to these large plagioclases (>10 mm), there is also a second population of smaller crystals (micro-phenocrysts). Small apatites are included in feldspars and clinopyroxenes.

PV-H forms a succession of massive lava blocks more than 90 m thick that rest against the southern summit of Pico Viejo volcano, interpreted as the remains of a lava lake (Ablay, 1997; Ablay and Martí, 2000). Its sample shows a crystal-rich trachytic texture (Figure 4B) with plagioclase (60.6%) Fe-Ti oxides (19.7%), and clinopyroxene (16.4%) with only 1.7% vesicles. It also contains small amounts of olivine (0.6%), and apatite as an accessory mineral within other phenocryst phases. Euhedral clinopyroxenes and oxides usually appear together in glomerocrysts.

Two phonolites were collected from the Teide central vent: Teide J2 is older and composed of several a'a, crystal-poor lava lobes with alkali feldspar phenocrysts (2.9%); (Figure 4C). Other minerals in this sample are biotite (0.3%), Fe-Ti oxides (0.1%), and trace clinopyroxene. Apatite also occurs

mostly as inclusions in other mineral phases. Groundmass (87.5%) is glassy with a significant amount of feldspar microlites and vesicles (9.2%). Lavas Negras is the last eruption of Teide volcano at ~ 1 ka (Carracedo et al., 2007; Brown et al., 2022). The sample was collected from a thick blocky lava flow between Teide and Pico Viejo and is characterised by a porphyritic texture in a dark-brownish glassy groundmass. The phenocryst assemblage is dominated by euhedral to subhedral alkali feldspar (21.9%), Fe-Ti oxides (1.5%), and clinopyroxene (0.9%). Some feldspar phenocrysts exhibit rounded textures with melt inclusions suggesting dissolution (Figure 4D). The groundmass (57.7%) has feldspar microlites that define a clear flow texture. The percentage of vesicles reaches 18% in thin section, and apatite occurs in both samples as an accessory mineral, mostly as inclusions.

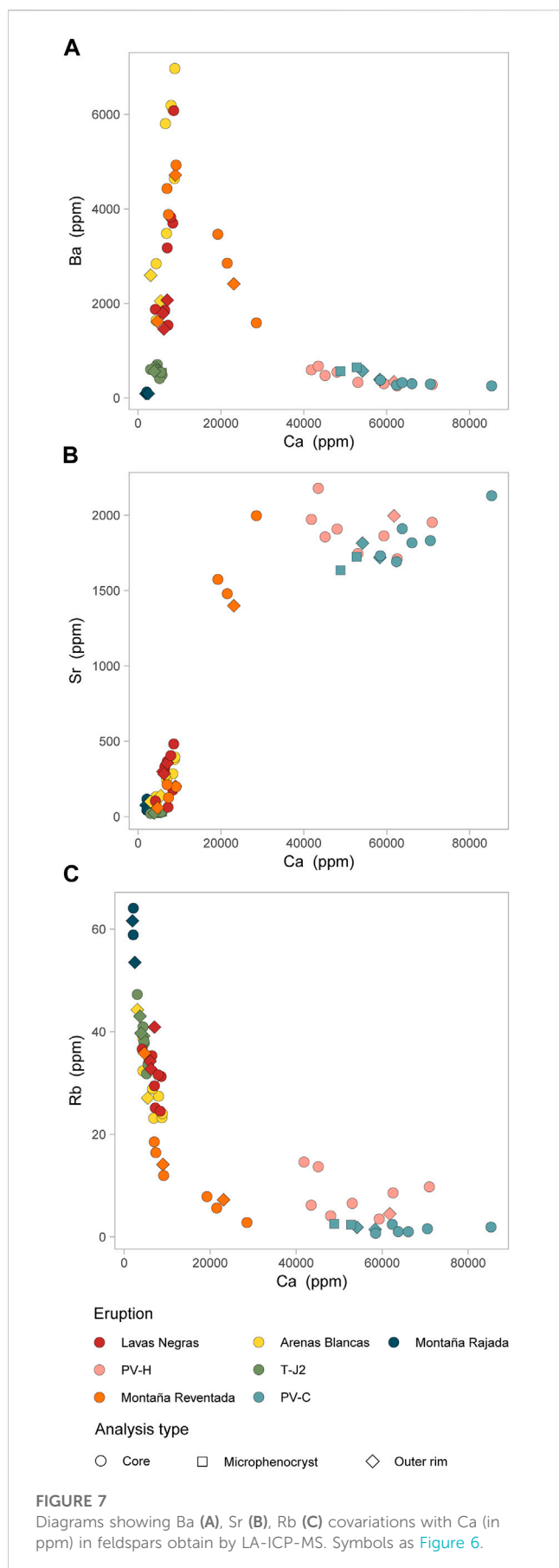
The other two phonolites, Arenas Blancas and Montaña Rajada, are both related to different subunits of the Montaña Blanca lateral vent (Ablay et al., 1995). Arenas Blancas is an older (4 ka) blocky lava flow containing a clear brownish glass (81%) with very few feldspar microlites and some vesicles (11.1%). The main phenocryst phase in Arenas Blancas is alkali feldspar (7.1%) and, to a lesser extent, biotite (0.3%),



Fe-Ti oxides (0.3) and clinopyroxene (0.2%); (Figure 4E). Montaña Rajada (2–4 ka) is an endogenous dome complex that belongs to the Lower Montaña Blanca member (Ablay and Martí, 2000) and its lavas are characterised by having only a small amount of alkali feldspar phenocrysts (0.7%) within a light coloured glassy matrix (79.7%) with feldspar microlites. It

also contains Fe-Ti oxides (0.2%) and biotite (0.1%) and has a fairly high percentage of vesicles (19.3%) (Figure 4F).

Sample ODG-20B (Figures 4G, H) is the upper trachyte member of Montaña Reventada. Montaña Reventada is a young (0.9–1.1 ka, Carracedo et al., 2007; Risica et al., 2020) fissure vent located on the west flank of Pico Viejo volcano, towards the Santiago del Teide rift



(Figure 1). It consists of a lower basanite layer and an upper trachyte lava flow that hosts common basanite inclusions (Ablay and Martí, 2000; Wiesmaier et al., 2011). The sample is porphyritic, with alkali feldspar (5.4%), Fe-Ti oxides (0.8%), biotite (0.4%), clinopyroxene (0.3%) and amphibole (0.2%). Both amphibole and biotite have dark reaction rims. Some feldspar phenocrysts show sieved textures (Figure 4G). The groundmass is vesicular (16.2%) and holocrystalline, consisting mainly of feldspar microlites and small Fe-Ti oxides and clinopyroxene.

4.3 Whole rock, glass, and mineral chemistry

4.3.1 Whole rock, glasses and groundmass

Rocks analysed in this work range from a phonotephrite to highly-evolved phonolites (Montaña Rajada, Lavas Negras, Arenas Blancas, and Teide J2). Montaña Reventada is classified as trachyte, but plots close to the phonolite field in Figure 3. In addition to whole rock analyses, electron microprobe analyses of groundmass glasses were also performed (Figure 3). Only four phonolites had glasses sufficiently free of microlites to be analysed.

Primitive mantle normalised trace element and REE plots (Figure 5) show enrichment in incompatible elements. Phonolites, especially the ones related to flank dome eruptions, are variably depleted in Ba, Sr, and Ti. The more evolved samples show positive spikes in Pb, Zr, and Hf. Europium is depleted in all phonolites ($\text{Eu}/\text{Eu}^* = 0.607\text{--}0.825$), while the less-evolved samples have essentially no Eu anomaly ($\text{Eu}/\text{Eu}^* = 1.012\text{--}1.039$). Notably, the Montaña Reventada trachyte has a positive anomaly ($\text{Eu}/\text{Eu}^* = 1.104$).

Glasses from T-J2, Lavas Negras, Montaña Rajada, and Arenas Blancas have similar normalised trace element and REE patterns with a relative enrichment in LREE over M-HREE and marked depletions in Ba, Sr, and Ti. All exhibit negative Eu anomalies ($\text{Eu}/\text{Eu}^* = 0.442\text{--}0.720$), especially Lavas Negras, Montaña Rajada and Teide J2. It is remarkable that, while the whole rock analysis of Lavas Negras has the least pronounced negative Ba anomaly of all phonolites analysed in this work (Figure 5A), its residual glasses are strongly depleted in Ba (Figure 5C).

4.3.2 Feldspar major and trace elements

Feldspar compositions vary continuously from bytownite in the phonotephrites to sanidine in the phonolites (Figures 2, 6, 7).

Plagioclase in the tephriphonolites shows a wide compositional range ($\text{Or}_{1-5}\text{Ab}_{25-55}\text{An}_{40-74}$ for PV-C and $\text{Or}_{1-10}\text{Ab}_{25-72}\text{An}_{17-74}$ for PV-H). In PV-C plagioclases, BaO and SrO analysed by EPMA range from 0 to 0.15 wt% and 0.3 to 0.4 wt% respectively (Figures 6B, C). PV-H plagioclases have wider ranges of Ba and Sr concentrations, with 0–0.6 wt% BaO and 0.2–0.5 wt% SrO (Figures 6B, C). PV-C feldspars analysed by LA-ICP-MS have Ba and Sr that range from 256 to 649 ppm and 1,635–2,130 ppm, respectively. Rb is very low in abundance, with values ranging from 0.7 to 2.6 ppm (Figure 7). PV-H feldspars have 259–674 ppm Ba and 1711–2,179 ppm Sr. Rubidium is also present in low abundances but with a wider range from 3 to 15 ppm (Figure 7).

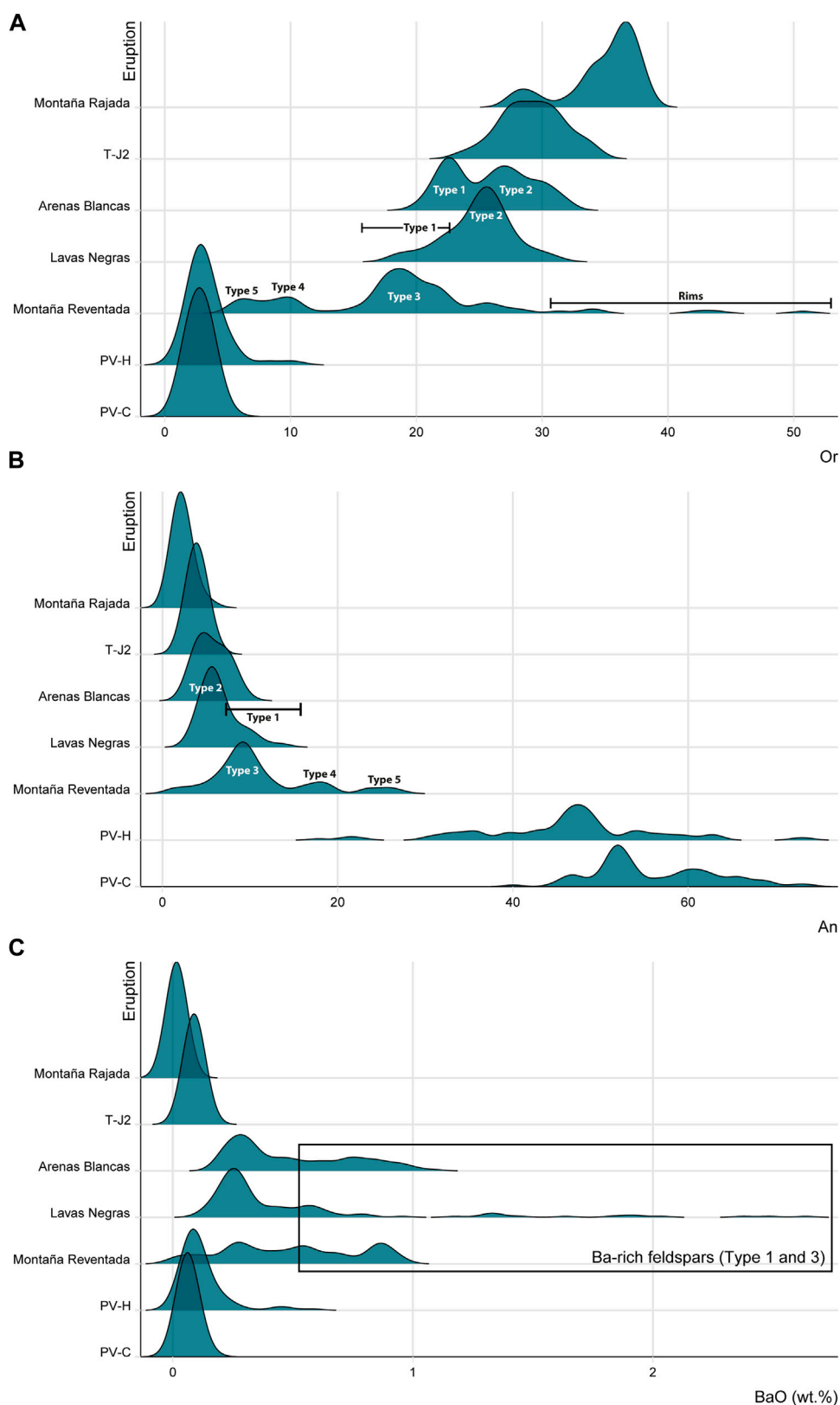


FIGURE 8 Probability density function plots of (A) Or, (B) An and (C) BaO (wt.%) of feldspar EPMA analyses, showing the data distributions for each eruption. Note multiple populations for the Lavas Negras, Arenas Blancas and Montaña Reventada eruptions.

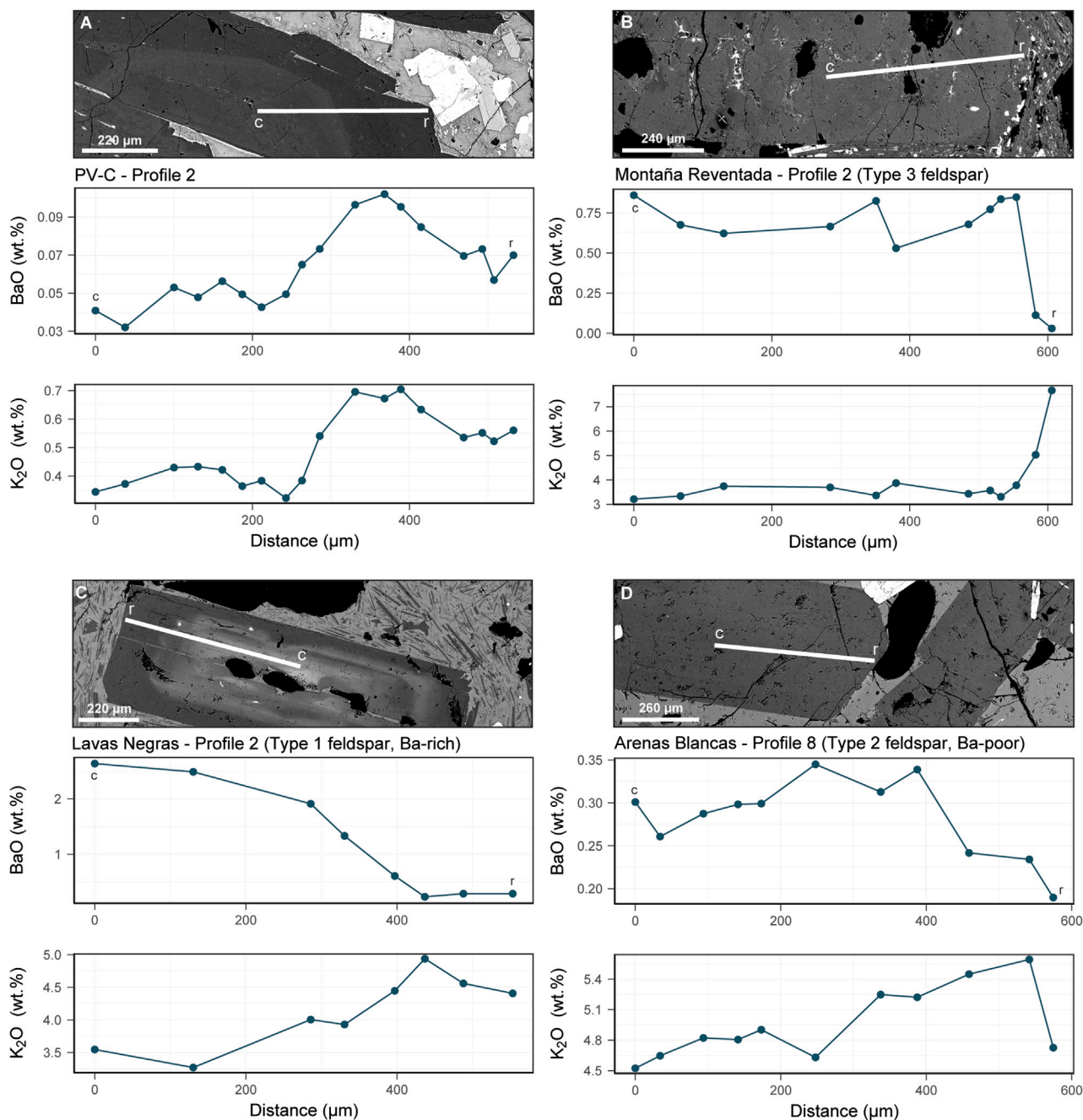


FIGURE 9

Zoning profiles showing compositional variations of BaO and K₂O (wt%) within representative feldspar phenocrysts in (A) PV-C; (B) Montaña Reventada (Type 1 feldspar); (C) Lavas Negras (Type 1 feldspar, with Ba-rich cores); (D) Arenas Blancas (Type 2 feldspar, with Ba-poor cores). The profile position is marked with a white line in accompanying back-scattered electron images.

In PV-C plagioclases there is a marked contrast between the composition of the phenocryst cores (Figure 4A), which show patchy zoning and higher An values (An₆₀₋₇₀), and rims of the phenocrysts and the microphenocrysts (An₄₅₋₅₅) (Figure 8). Some rims and microphenocrysts also show oscillatory zoning (Figures 4A, 9A). PV-H plagioclases exhibit a wider variation in chemical compositions towards slightly more evolved compositions (Figures 6, 8). In cores, the main population is ~An₄₇ (Figure 8),

with rims and microlites having more evolved compositions (~An₃₅, with up to 10% Or). In both tephriphonolites, Ba is enriched in feldspar rims (Figure 9A) and shows a clear negative correlation with An content, with phenocryst rims and microphenocrysts enriched in Ba (Figures 4B, 6B). No significant differences in the amount of Sr and Rb were observed between the cores and the rims.

Among the phonolites, the Teide J2 and Montaña Rajada eruptions show relatively homogeneous feldspar populations,




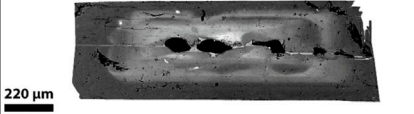
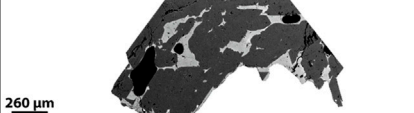
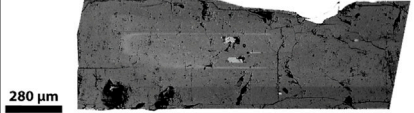
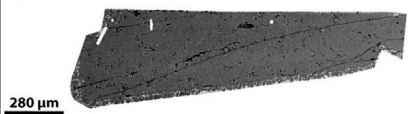
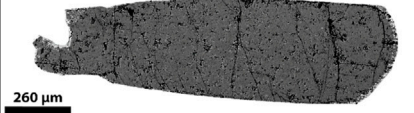

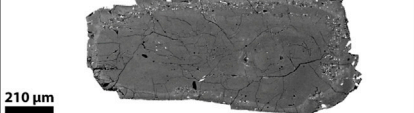
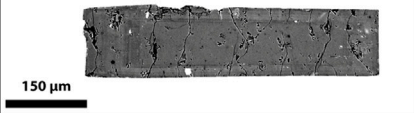
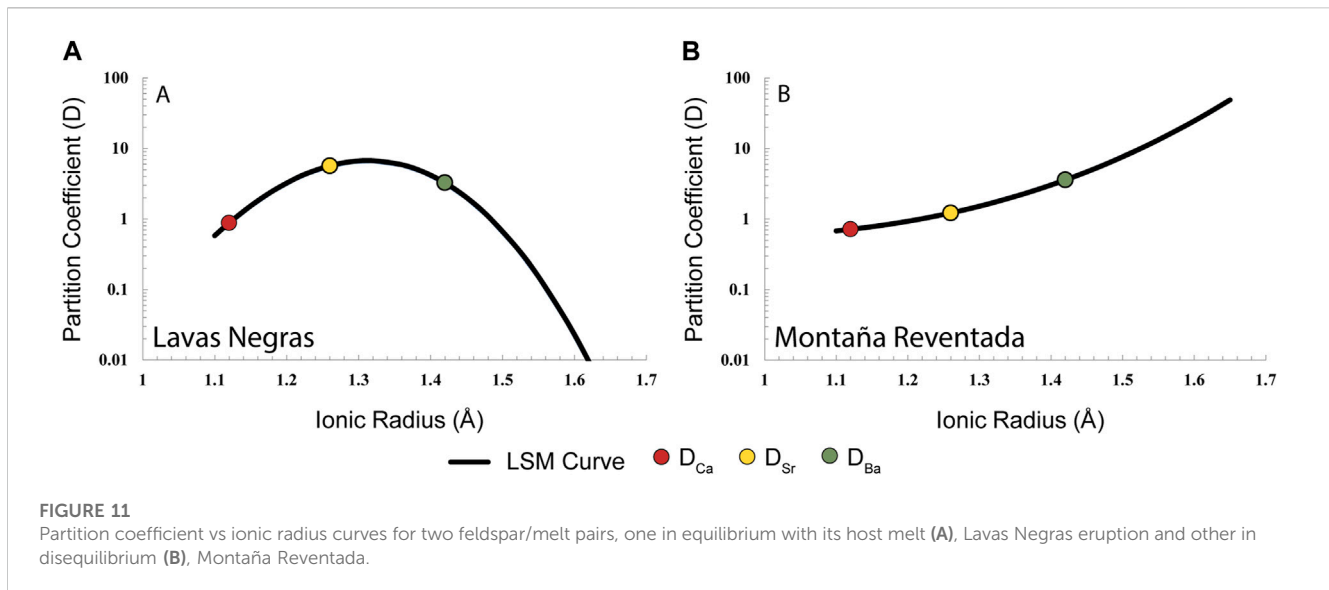
Eruption	Population Type	Representative Image	Population main chemical composition
PV-C	-		- Cores: 2 wt.% Or, 30-40 wt.% Ab and 60-70 wt.% An. - Rims and microphenocrysts: 3-4 wt.% Or, 45-50 wt.% Ab and 45-55 wt.% An.
PV-H	-		- Cores: 3 wt.% Or, 50 wt.% Ab and 47 wt.% An. - Rims and microlites: 5 wt.% Or, 60 wt.% Ab and 35 wt.% An.
T-J2	-		- Cores: 29 wt.% Or, 67 wt.% Ab and 4 wt.% An. - Rims: slightly more enriched in Or.
Lavas Negras	Type 1		- Cores: 23 wt.% Or, 67 wt.% Ab and 10 wt.% An. BaO up to 2.6 wt.%. - Rims: 25 wt.% Or, 69 wt.% Ab and 6 wt.% An.
	Type 2		- Cores: 26.5 wt.% Or, 68.5 wt.% Ab and 5 wt.% An. BaO up to 0.6 wt.%. - Rims: 25 wt.% Or, 69 wt.% Ab and 6 wt.% An.
Arenas Blancas	Type 1		- Cores: 22.5 wt.% Or, 70 wt.% Ab and 7.5 wt.% An. BaO up to 1.1 wt.%. - Rims: 29 wt. Or, 67 wt.% Ab and 4 wt.% An.
	Type 2		- Cores: 29 wt.% Or, 67 wt.% Ab and 4 wt.% An. BaO up to 0.5 wt.%. - Rims: 29 wt. Or, 67 wt.% Ab and 4 wt.% An.
Montaña Rajada	-		- Cores: 36 wt.% Or, 62 wt.% Ab and 2 wt.% An. Only one core slightly enriched in Ab (up to 67 wt.%). - Rims: same as cores.
Montaña Reventada*	Type 3		- Cores: 19 wt.% Or, 72 wt.% Ab and 9 wt.% An. BaO up to 1 wt.%. - Rims: 30-50 wt.% Or, 50-65 wt.% Ab and 1-5 wt.% An.
	Type 4		- Cores: 9 wt.% Or, 73 wt.% Ab and 18 wt.% An. BaO up to 0.6 wt.%. - Rims: 30-50 wt.% Or, 50-65 wt.% Ab and 1-5 wt.% An.
	Type 5		- Cores: 6 wt.% Or, 69 wt.% Ab and 25 wt.% An. BaO up to 0.3 wt.%. - Rims: 20 wt.% Or, 73 wt.% Ab and 6 wt.% An.

FIGURE 10

Table illustrating the population of feldspar phenocrysts found in Teide-Pico Viejo samples. *Type 4 and 5 cores in Montaña Reventada grade into compositions similar to Type 3 cores towards the outer part of the mineral. See text and [Figure 9](#).



while Lavias Negras and Arenas Blancas show multiple populations (Figures 8, 10). Teide J2 feldspars are anorthoclases ($Or_{23-34}Ab_{63-71}An_{3-6}$) and have BaO and SrO concentrations as follows: Ba, 412–708 ppm; Sr, 21–47 ppm; Rb, 32–47 ppm (Figures 4C, 7). In this sample, rims are slightly more enriched in Or, with a subtle positive correlation with Ba. In Montaña Rajada, feldspars are classified as anorthoclase and sanidine ($Or_{28-38}Ab_{61-69}An_{2-5}$). LA-ICP-MS analyses returned values of 92–126 ppm Ba, 36–117 ppm Sr, and 54–64 ppm Rb (Figure 7). The majority of feldspars in this sample show no significant zonation (Figure 4F), with only one crystal showing slightly higher Ab in its core.

Lavias Negras (TL) and Arenas Blancas both have two distinct feldspar populations (Figures 8, 10). Overall, their feldspars are classified as anorthoclase ($Or_{18-31}Ab_{65-72}An_{3-14}$ for Lavias Negras and $Or_{20-32}Ab_{65-71}An_{3-9}$ for Arenas Blancas). Feldspars from Lavias Negras have extremely high BaO concentrations, reaching 2.6 wt%, with minimum values of 0.1 wt% (Figure 6B). SrO ranges from below detection limit to 0.21 wt% (Figure 6C). Ba, Sr, and Rb measured by LA-ICP-MS range from 1,458 to 6,079 ppm, 63–482 ppm, and from 25 to 41 ppm, respectively (Figure 7). Some Arenas Blancas feldspars are also enriched in Ba (Figure 6B) but don't reach such extreme values as in Lavias Negras lava flow. In Arenas Blancas feldspars, BaO, and SrO range from 0.2 to 1.1 wt% and from below detection to 0.1 wt%, respectively (Figures 6B, C). LA-ICP-MS analyses yield 1,636–6,970 ppm of Ba, 93–394 ppm of Sr and 23–44 ppm of Rb (Figure 7). In both samples, two feldspar populations can be clearly distinguished (Figures 8, 10): The first (Type 1 feldspars) is characterised by extremely BaO-enriched cores (Figures 8B, 9C). These cores are also the least evolved, with BaO being positively correlated with An over the range An_{8-14} (Figure 6B). This population is also characterised by oscillatory zoning and resorbed cores (Figures 4D, E).

The second population of feldspar (Type 2) has cores that are less enriched in BaO (up to 0.6 wt%). Type 2 is the dominant population in both samples, with compositions $Or_{26-30}Ab_{66-88}An_{3-7}$ (Figure 8). Both Type 1 and 2 feldspars

share the same rim compositions, more similar to that of the Type 2 feldspar cores, but slightly depleted in BaO and Or. In Type 1 feldspars, BaO strongly decreases from core to rim (Figure 9C), while in Type 2 it decreases with a much less marked variation or remains more or less stable (Figure 9D). The amount of Or sharply decreases towards the outer rims in some feldspars (Figure 9D). In Type 1 feldspars, strontium shows, along with BaO, a clear decrease from core to rim (Figures 4D, E). However, the opposite trend is observed in Type 2 feldspars, where a slight increase in the amount of Sr towards the rim is observed. No clear trends in Rb are observed in either group. Also, two types of microlites are present in Lavias Negras. One has compositions similar to the phenocryst rims and the other is richer in CaO. The latter group exhibits the lowest values for BaO, and is more enriched in FeO (~0.45 wt%, Figure 6).

Montaña Reventada feldspars exhibit a wide range from $Or_6Ab_{67}An_{27}$ to $Or_{51}Ab_{48}An_1$ (Figures 2, 8). The amount of BaO and SrO in these samples ranges from below EPMA detection limit to 1 wt% and from below detection limit to 0.38 wt%, respectively (Figures 6B, C). The LA-ICP-MS concentration range is from 1,589 to 4,927 ppm of Ba, 58–1997 ppm of Sr, and 3–36 ppm of Rb (Figure 7). In Montaña Reventada, the main core population has $Or_{19}Ab_{72}An_9$ (Type 3), but less abundant populations are also observed at $Or_9Ab_{73}An_{18}$ (Type 4) and $Or_6Ab_{69}An_{25}$ (Type 5) (Figures 8, 10). Type 3 feldspars showed the most Ba-rich and Sr-poor cores in Montaña Reventada (from 0.6 to 1 wt% and from 0 to 0.1 wt%, respectively, Figure 8). Type 4 and 5 are progressively less enriched in BaO and more enriched in SrO and have lower Rb concentrations. Type 4 and 5 feldspars also show greater textural evidence of disequilibrium, with sieved textures and resorbed rims and overgrowths (Figure 4G). Rims of Montaña Reventada feldspars have up to Or_{50} , with An always less than 6 wt%. These rims are also depleted in BaO (normally less than 0.25 wt%, Figure 9B) and Sr (58–201 ppm except the rim of Type 5 feldspar, with 1,399 ppm), with variable amounts of Rb (from 7 to 36 ppm). It is important to note that towards the rims, feldspars with Type 4 and 5 cores acquire a similar composition to Type 3 feldspar cores before the latest

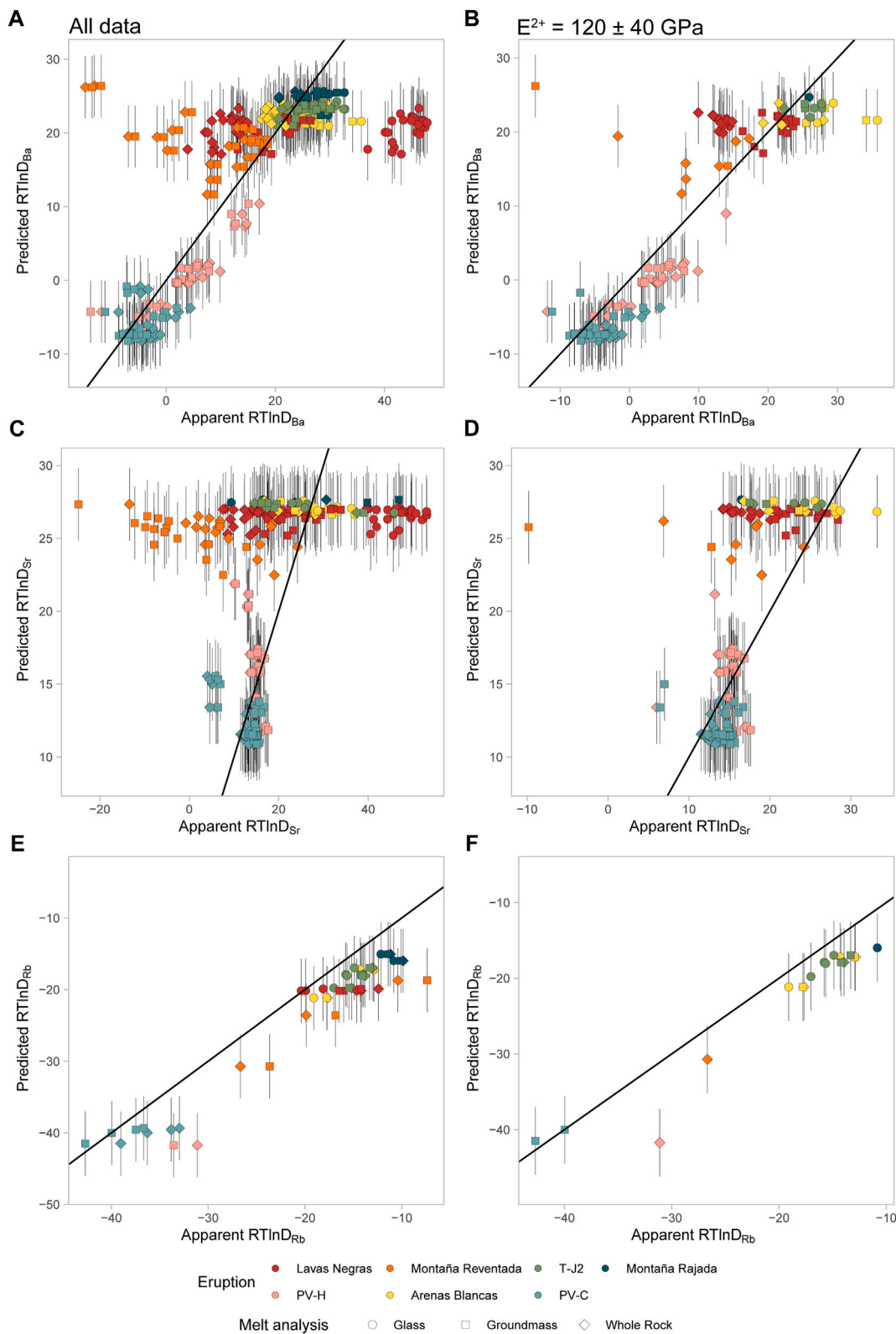


FIGURE 12

Diagrams showing $RTInD_{Ba}$, $RTInD_{Sr}$ and $RTInD_{Rb}$ predicted from Eqs 1–3, respectively, compared to observed values in T–PV samples. Thick black lines are the one-to-one correlation. Thin lines are error bars calculated by the model (± 4.216 for $RTInD_{Ba}$, ± 4.498 for $RTInD_{Sr}$ and ± 4.670 for $RTInD_{Rb}$). (A), (C), (E) All D values calculated in this work. (B), (D), (F) Only mineral–melt pairs with an E^{2+} value in the range of 80–160 GPa. Note that in some cases Sr is below detection in EPMA analyses, and therefore is not represented in these panels.

TABLE 2 Table showing a summary of the theoretical D_i ranges calculated by equations E1, E2, and E3 for each Teide-Pico Viejo eruption studied in this work, as well as the predicted quantities of Ba, Sr, and Rb that feldspars in equilibrium with the whole rock composition should contain.

Eruption	Theoretical D calculated by equations E1, E2, and E3						Theoretical amount of Ba, Sr, and Rb in feldspars (in ppm)					
	Minimum DBa	Maximum DBa	Minimum DSr	Maximum DSr	Minimum DRb	Maximum DRb	Minimum Ba	Maximum Ba	Minimum Sr	Maximum Sr	Minimum Rb	Maximum Rb
Montaña Rajada	11.02	15.56	17.84	19.30	0.15	0.25	82.08	103.70	32.17	33.72	26.89	45.86
TJ2	9.15	12.80	16.65	17.90	0.12	0.20	442.62	567.21	59.48	62.30	20.10	34.56
Arenas Blancas	8.48	11.48	15.16	16.65	0.12	0.20	1,517.81	1785.36	128.86	134.03	20.48	34.84
Lavas Negras	5.42	10.00	12.02	14.60	0.09	0.19	1,588.54	1877.32	409.69	423.60	16.01	33.52
Montaña Reventada	3.15	13.40	9.13	14.71	0.05	0.45	3,181.30	8,579.09	1,296.28	1,690.44	5.18	46.78
PVH	0.52	2.67	3.03	7.90	0.02	0.05	769.98	1,371.03	1,520.51	1,699.09	3.68	10.65
PVC	0.46	0.93	2.80	4.34	0.02	0.02	474.04	837.70	2,145.77	2,625.63	1.28	1.86

abrupt increase in Or. All analysed crystals have a progressive rimward decrease in Ba and Sr (Figures 4H, 9B). No clear trends in Rb concentrations from cores to rims are observed. Microlites also show a wide compositional range, although most of them have major element compositions that overlap with phenocryst rims.

4.3.3 Measured crystal/matrix concentrations for Rb, Sr and Ba in natural samples

We have calculated the apparent partition coefficient (D) using EPMA (for Ba and Sr) and LA-ICP-MS (for Ba, Sr, and Rb) feldspar analyses. For the melt composition, we calculate different D values using both the compositions of the whole rock and glasses. In addition, we also calculate the D for the feldspar/groundmass composition using analyses obtained by Brown et al. (2022) and Ramos et al. (in prep). For samples in which groundmass analyses were not available, estimated compositions have been obtained by mass balance using the compositions of the whole rock, the compositions of the main mineral phases, and their modal percentages. Temperatures used in the calculations were obtained using the experimentally-derived melt composition geothermometer for phonolites derived by Martí et al. (2020), which is calibrated specifically for the evolved magmas of Tenerife. For the less evolved compositions, we used the temperatures obtained by Ablay (1997).

To assess the calculated coefficients, the distribution coefficients of Ca, Ba, and Sr were used to construct “Onuma” curves of D vs ionic radius (Onuma et al., 1968) and the corresponding value of the divalent cation site elastic modulus, E^{2+} , was calculated (Blundy and Wood, 1994; Figure 11). Acceptable values for this parameter for divalent cations in alkali feldspar, derived from feldspar/melt partitioning experiments (Long, 1978; Icenhower and London, 1996; Fabbrizio et al., 2009), lie in the range 120 ± 40 GPa (Brown et al., 2022). In Figure 12, calculated D values for Sr, Ba, and Rb are compared with phenocryst/melt results for all pairs (Figures 12A, C, E), and for those that pass the $E^{2+} = 120 \pm 40$ GPa filter (Figures 12B, D, F).

The values of D_{Ba} measured on all samples that pass the test for equilibrium range from 0.3 to 38.3, with the highest values found in the phonolites. D_{Sr} ranges from 0.4 to 29.7 while Rb is always incompatible, with D_{Rb} between 0.02 and 0.31. Note that these

coefficients only correspond to mineral/melt pairs at equilibrium that have been calculated using three different types of melt compositions (whole rock, groundmass and glass). PV-C and PV-H feldspar rims all appear to show equilibrium partitioning with both whole rock and groundmass compositions. Rims of Lavas Negras feldspars are also in equilibrium with the whole rock and also with the groundmass analyses. On the other hand, T-J2 is mostly in equilibrium with the average glass composition, but some of them are also in equilibrium with groundmass and the whole rock. Montaña Rajada and Arenas Blancas rims may be in equilibrium with the three types of melts. Lastly, Montaña Reventada feldspar rims are mostly in equilibrium with the whole rock but some of them are also in equilibrium with the groundmass.

5 Discussion

5.1 Comparison of calculated and observed D values to Teide-Pico Viejo lavas

We have attempted to derive expressions for Ba, Sr and Rb partition coefficients that apply to the entire compositional range of feldspars in alkaline magmatic systems, from anorthite to sanidine. Using the experimental data available in the literature, we found an equation to predict the partition coefficients for these three elements (Eqs 1–3). Results are particularly good for D_{Ba} and D_{Rb} , with R^2 values above 0.95. In the case of D_{Sr} , the fit is still fairly good, albeit with an R^2 value that is significantly lower (0.902) than that achieved with the other two trace elements.

The predicted $RT \ln D_i$ for the three elements show patterns consistent with the lattice strain model (Blundy and Wood, 1994). Partition coefficients for Ba and Rb increase with decreasing An and increasing Or content of the feldspar, whereas Sr shows more complex behaviour. A linear relationship was found between $RT \ln D_i$ and An, and a logarithmic relationship with respect to the amount of Or for Ba and Rb. These behaviours arise because the ionic radii of Ba and Rb are greater than the host lattice site size range in plagioclase and most alkali feldspar, whereas that of Sr lies within the range in alkali feldspar. Thus, $\ln D_{Sr}$ peaks at about Or₃₀ and cannot be expressed as a

monotonic function over the compositional range of interest. The maximum and minimum theoretical D_i values obtained in the feldspars of each of the eruptions are listed in Table 2.

Figure 12 shows a comparison between real $RT\ln D_i$ values measured in the natural samples compared to model predicted values for Ba, Sr and Rb. Note that only mineral-melt pairs with an E value in the range of 80–160 GPa are plotted in Figures 12B, D, F. Those that do not meet this condition are considered to be out of equilibrium. In most of the studied units, the majority of feldspar rims are close to trace element equilibrium with the host melt, especially when the partition coefficients are calculated with the whole rock and groundmass analyses. Only the more evolved samples with lower crystallinity (e.g., T-J2 and Montaña Rajada) are found to be in equilibrium with the glasses analysed.

The model works well (within the margin of error) in predicting D_{Ba} in most of the samples analysed, with the exception of most feldspars from Montaña Reventada (Figure 12B). In most cases the fit is better if the groundmass is used as the melt value to perform the calculations. The only two exceptions are the Montaña Rajada and Arenas Blancas cases, where using the average of the glass analysis and the whole rock, respectively, gives a better fit to the 1:1 line. As expected, the D_{Sr} model clearly gives the worst results when applied to T-PV lavas (Figure 12D) since, as previously discussed, this element could not be successfully modelled. And finally, regarding Rb, our expression generally succeeds in predicting $RT\ln D_{Rb}$ although a slight underestimation has been observed especially in the more evolved compositions (Figure 12F).

5.2 Origin of phenocrysts and interpretation of magmatic processes

5.2.1 Identification of xenocryst populations within T-PV lavas

Knowing the whole rock concentration of a trace element “i” and the theoretical D_i calculated from the model, it is possible to predict the concentration of this element in the groundmass and in the crystal for any crystallinity of the sample according to the following expressions:

$$C_{WR} = (X_{xt} * C_{xt}) + (X_{gm} * C_{gm}) \quad (4)$$

$$X_{xt} = 1 - X_{gm} \quad (5)$$

$$D = \frac{C_{xt}}{C_{gm}} \quad (6)$$

Where C is the concentration of the element “i” and X is the mass fraction of the whole rock (WR), crystal (xt), and groundmass (gm). Using the minimum and maximum D_i values calculated from the model to the analyses in the sample and the percentage of feldspar minerals present in the sample, we are able to obtain the theoretical amount of Ba, Sr, and Rb that the feldspars should have if they were, in fact, cognate with the whole rock composition (Table 2). We focus mostly on Ba due to its wide variations and better partitioning model quality than Sr.

In the mafic and intermediate samples PV-C and PV-H, feldspar cores are moderately enriched in Ba relative to values predicted from their host magma compositions. This result is not unexpected,

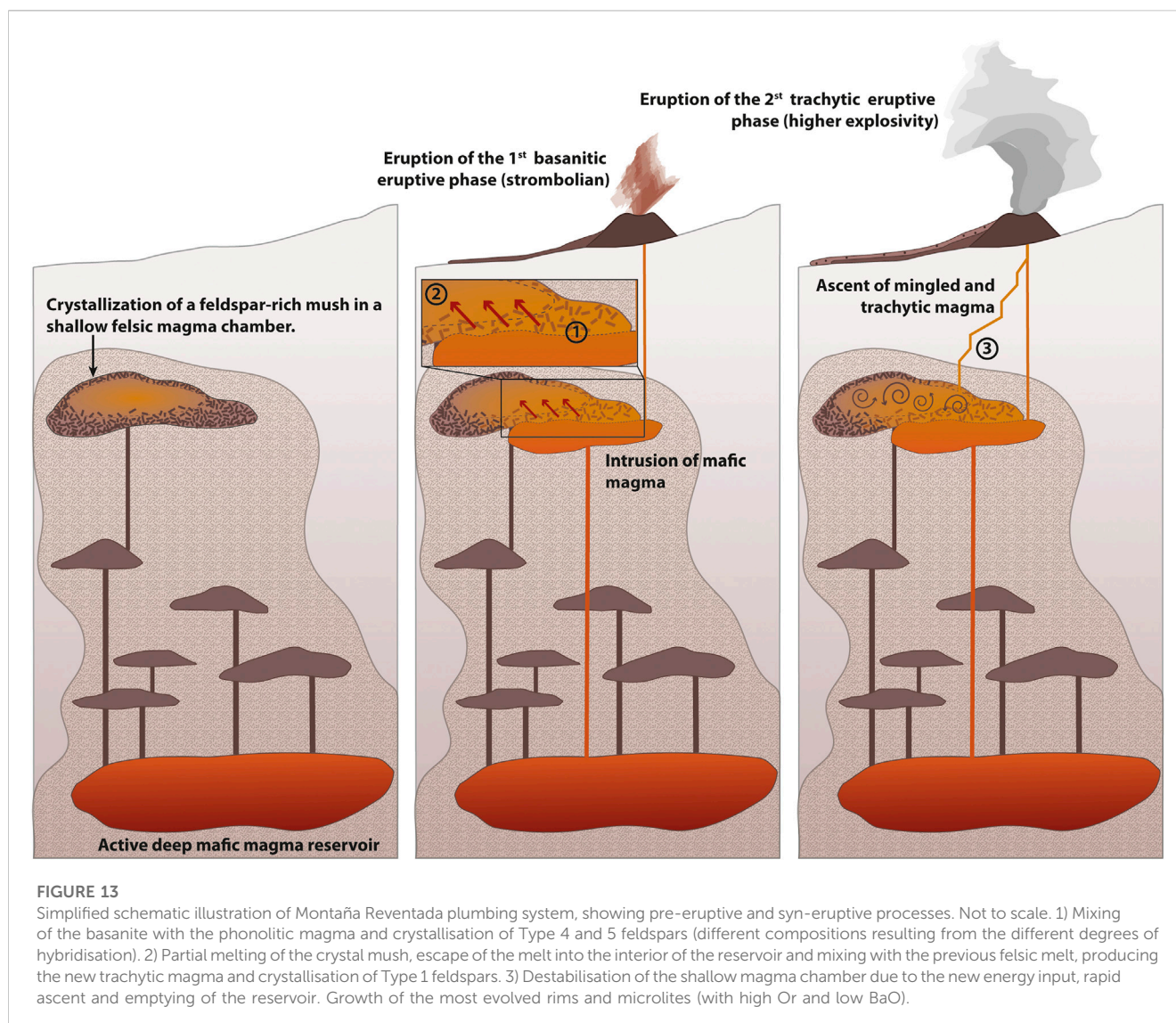
particularly in PV-C, given clear textural evidence of disequilibrium such as resorbed, cellular texture cores with patchy zoning surrounded by a more evolved mantle (Figures 4A, 9A). In PV-H, a more gradual core-rim shift is observed (Figure 4B). The smaller size and presence of some textures derived from skeletal growth in the most evolved feldspar population in PV-C (particularly in microphenocryst and microlites; Figure 4A) could result from rapid decompression and volatile loss (Giacomoni et al., 2014).

Most of the feldspar phenocrysts in the phonolites show equilibrium or near-equilibrium partitioning of Ba with the final melt with the exception of Type 1 (Ba-rich) feldspars in Lavas Negras and Arenas Blancas eruptions and most of the Montaña Reventada feldspars (especially those of Type 4 and 5, the less evolved feldspars in the sample).

Type 2 feldspar cores and rims in Lavas Negras and Arenas Blancas appear to be cognate to their host magmas. In contrast, Type 1 feldspar cores have abnormally high Ba contents (up to more than 2 wt% in the more extreme cases of Lavas Negras; Figure 8B). This feldspar population also show a slightly higher concentration Sr, but do not reach the levels found in the phonotephrites. These minerals also show the greatest discrepancy between measured and predicted D values in some of the rims, and partition coefficients for divalent cations do not define parabolic Onuma curves. All of these features provide a means of assessing disequilibrium of these minerals with their host magma. This may be evident in those minerals that show clear textural evidence of disequilibrium, such as dissolved cores and corrosion re-entrants (Figures 4D, 9C, 10) but less so in those minerals that are also Ba-enriched and yet have near-euhedral shapes and textures similar to those of Type 2 feldspars (Figures 4E, 10). Without partitioning information, the latter could pass for simple phenocrysts and lead to misinterpretations as to their antecrystic or xenocrystic origin.

Type 1 feldspar compositions (maximum An_{14}) rule out an origin from less evolved magmas similar to those of PV-C and PV-H. Nonetheless, it is evident that these alkali feldspars formed in magmas that were somewhat less evolved than those that gave rise to the Type 2 feldspars. If we calculate the theoretical amount of Ba for their cogenetic melt we get a maximum of 1,250 ppm for Arenas Blancas and more than 4,000 ppm for Lavas Negras. The latter is much higher than in any recent volcanic product of Tenerife (Ridley, 1970; Araña et al., 1989; Araña et al., 1994; Balcells and Hernández-Pacheco, 1989; Fernández Satín and Vicente-Mingarro, 1989; García Moral, 1989; Ovchinnikova et al., 1995; Ablay, 1997; Neumann et al., 1999; Rodríguez Badiola et al., 2006; Wiesmaier et al., 2011; García et al., 2012; Albert et al., 2015a; di Roberto et al., 2016).

All these features suggest that these feldspars formed likely in a cumulate mush zone, as proposed by D’Orsiano et al. (2017) in generating some feldspars in the Lajes Ignimbrite trachyte (Terceira Island, Azores). Occasional feldspar aggregates in both samples support this hypothesis. Disequilibrium textures and patchy and/or oscillatory zoning in some of these feldspars suggest multiple melting and crystal re-growth events, processes which are favourable for generating strongly Ba-enriched feldspars (Wolff et al., 2020). Local melting of part of this feldspar-dominated cumulate and recrystallisation from the resultant Ba-enriched liquids is a possible explanation for forming “Type 1” feldspars. These findings are in line with those found by Ablay et al. (1998) for



Lavas Negras eruption. Also, consistent with these observations, [Brown et al. \(2022\)](#) report that both Lavas Negras and Arenas Blancas each host two feldspar populations, 1) phenocrysts in equilibrium with the enclosing melt phase, and 2) older feldspars interpreted as either xenocrysts introduced during assimilation of pre-existing rocks or antecrysts derived from a crystal-rich mush reservoir.

Crystal dissolution can be caused by magma mixing with more primitive magmas (e.g., [Sundermeyer et al., 2020](#)), H₂O-undersaturated decompression (e.g., [Humphreys et al., 2006](#)) or melt temperature changes (e.g., [Bachmann and Bergantz, 2006](#)). No evidence of significant magma mixing between the phonolitic magma and a basanitic/intermediate magma have been found in either Lavas Negras or Arenas Blancas eruptions and melting caused by magma ascent alone cannot explain the accumulation of such enriched melts in Ba. For this reason, we argue that dissolution of this feldspar cumulate is most likely due to a temperature rise caused at the bottom of the reservoir by the intrusion and underplating of hotter magma ([Couch](#)

[et al., 2001](#); [Wolff et al., 2015](#); [D'Oriano et al., 2017](#); [Landi et al., 2019](#)). Processes like this have been previously documented for other eruptions in the T-PV volcanic complex (e.g., Pico Cabras dome eruption, [Dorado et al., 2021](#)).

Both Lavas Negras and Arenas Blancas samples lack a positive Eu anomaly, but this fact alone should not be taken as evidence against feldspar accumulation, or fusion of the crystal mush, since if the magma is highly fractionated, the incorporation of feldspar cumulates and/or the fusion of such may not be sufficient to erase the previous negative Eu anomaly ([Wolff et al., 2020](#)). Therefore, for a correct interpretation of these anomalies it is necessary to also consider chemical data and observations at the crystal scale. Notably, the Eu anomalies in both samples are larger in the residual glasses than in their whole rock analyses (particularly in Lavas Negras, with $\text{Eu}/\text{Eu}^* = 0.45\text{--}0.52$ in residual glass and 0.82 in whole rock). All these features allow us to hypothesize that the dissolution-crystallisation processes were very localized within the crystal mush in a poorly mixed system in which those melts didn't communicate with the rest of the magmatic system, and only a

fraction of this crystal mush could be remobilised and incorporated into the juvenile magma during the destabilization of the magma chamber prior to eruption.

Another eruption that retains multiple feldspar populations that record complex magmatic evolution is Montaña Reventada. It has three different feldspar core compositions (Figure 10) all of which show increasing Or towards the rims of the phenocrysts, accompanied by decreasing Ba abundances. Most of the analysed feldspars rims exhibit large discrepancies between measured and predicted D (Figure 12), and do not yield upward-convex parabolic $\ln D$ -ionic radius relations (Figure 11B) expected of equilibrium crystal/melt pairs.

Texturally, Montaña Reventada feldspars with Type 4 and 5 cores show greater signs of disequilibrium (e.g., sieved textures, reabsorbed rims and overgrowths; Figures 4G, 10). Both types contain the least-evolved feldspars in the sample, with Ca contents up to An_{27} . The predicted equilibrium Ba contents of the magma from which these feldspars originate lie between 1,250 and 1,700 ppm, which correspond to those obtained from many PV-C and PV-H (phonotephrites) phenocrysts. Compared to major elements, these feldspars have compositions almost overlapping the PV-H phenocryst rims. Previous studies performed on Montaña Reventada products (Araña et al., 1994; Wiesmaier et al., 2011) have identified enclaves and inclusions of phonotephrite. Therefore, such feldspars may be the product of those mafic/intermediate composition magmas that entered the evolved reservoir during the magma mixing event.

Ba concentrations in Montaña Reventada Type 3 feldspars are highly variable. Based on our Ba partitioning model, only feldspars with 0.6–0.8 BaO wt% are in equilibrium with their host magmas. Higher Ba values have also been found in Type 3 feldspar cores, originating from evolved magmas with Ba up to 1,600 ppm. Orthoclase (Or) contents increase towards the rims of the feldspars, accompanied by a rapid decrease in Ba. This Or-rich and Ba-poor composition, which is also found in the microlites, is notable for being in equilibrium with magmas that are more heavily depleted in Ba (from 0 to 1,000 ppm) than those suggested by both the whole rock and groundmass.

5.2.2 Evidence of cumulate melting in Montaña Reventada eruption products

Multiple lines of evidence of cumulate/crystal mush melting have been identified in Montaña Reventada volcanic products. This eruption extruded less SiO_2 -undersaturated magma (trachyte rather phonolite), with low Zr, high Ba, and Sr, and a positive Eu anomaly. These are clear indicators for the partial melting of an alkali feldspar-rich mush, as reported extensively in the literature (e.g., Sliwinski et al., 2015; Wolff, 2017; Astbury et al., 2018; Wolff et al., 2020; González-García et al., 2022). Figure 3 shows how the whole rock composition of Montaña Reventada deviates from phonolite towards alkali feldspar.

However, the melting of a feldspar crystal mush is often accompanied by the formation of reversely zoned, Ba-enriched rims in feldspars (Bachmann et al., 2014; Wolff et al., 2015, 2020; Foley et al., 2020), a feature not observed in the analysed Montaña Reventada feldspars. However, we do observe Ba-rich feldspar cores (Type 3) with oscillatory zoning with some bands more enriched in Ba (lighter bands in Figure 4H) before

the outward decrease in Or and Ba to the outer rim. Continuing crystallisation also results in Ba-poor feldspars due to the depletion of Ba in the melt.

A possible explanation for the Montaña Reventada plumbing system (Figure 13) and the processes that preceded the eruption are:

- 1 Intrusion of mafic magma into a pre-existing, evolved magma chamber, with a crystal-rich cumulate zone at the bottom of the reservoir. Mixing between the magma of the mafic intrusion and the stored magma results in the crystallisation of less evolved feldspars (Type 4 and 5), with compositions consistent with their origin in a tephriphonolitic magma. Part of this magma continues to ascend to the surface leading to the first basanitic phase of the eruption (Araña et al., 1994; Wiesmaier et al., 2011; Albert et al., 2015b).
- 2 The rise in temperature caused by this intrusion led to widespread melting of the crystal mush, which mixed with the original magma to produce a trachyte, displaced to a slightly more mafic composition (Figure 3). From this new magma, Type 3 feldspars grew along with the regrowths found in Type 4 and 5 feldspars with more or less Ba depending on the extent of crystallisation and whether the magma zone in which they crystallised is more or less affected by the mush partial melt.
- 3 The rapid crystallisation of these phenocrysts, perhaps associated with rapid ascent, causes a sudden evolution of the residual magma and depletion in Ba and Sr, as reflected in the feldspar outer rims.

Mafic recharge leading to partial melting and remobilisation of a feldspar-rich crystal mush has been previously documented in Tenerife but only for Las Cañadas Edifice eruptions (Sliwinski et al., 2015; González-García et al., 2022). This is the first time that this type of magmatic process has been proposed in the T-PV active system. Also noteworthy is the presence of banded pumice in the Montaña Reventada eruption deposits, very similar to those described in El Abrigo and several other units of the Diego Hernández Formation (Edgar et al., 2002; Pittari, 2004; Edgar et al., 2007; Edgar et al., 2017; González-García et al., 2022). All of these characteristics are further evidence that the T-PV volcanic system is beginning to reveal its capacity for magma-magma interactions leading to highly explosive eruptions, similar to those of previous volcanic cycles of the Las Cañadas Edifice.

6 Conclusion

We provide expressions that adequately model partition coefficients between the whole feldspar compositional range and melt for Ba, Sr, and Rb using experimental data available in the literature. These expressions provide a working description of the feldspar compositional dependency of mineral/melt partitioning of these elements. We show that comparison of predicted and measured/apparent partition coefficients in volcanic rocks provides a way of tracking magmatic processes. Due to relatively high abundance enabling accurate analysis, and strong partitioning into feldspars of most interest here (sodic plagioclase through anorthoclase), Ba has proven to be the element best suited as an

indicator for relationships between feldspar and its carrier melt as well as for tracking magmatic fractionation processes, cumulate formation and remobilisation.

We apply these expressions to samples from the basanite-phonolite suite of the Teide-Pico Viejo volcanic system (Tenerife, Spain). Using differences between the measured and predicted partition coefficients, we are able to distinguish between different feldspar populations (phenocrysts, xenocrysts and antecrysts) in the Lavas Negras, Arenas Blancas, and Montaña Reventada eruptions. In addition, we use predicted D values to calculate the theoretical Ba content of the magmas in which the feldspars crystallised, which provide important clues about the petrogenesis of the different chemical populations. This makes it possible to identify a population of feldspars of cumulate origin in Lavas Negras and Arenas Blancas eruptions that had undergone multiple disequilibrium (fusion) and re-equilibration (recrystallisation) events due to reheating of the magma chamber. Clear evidence of cumulate melting as the origin of the Montaña Reventada trachytic magma was also found. The application of these techniques to active magmatic systems allows detailed characterisation of pre-eruptive magmatic processes, with implications for volcanic eruption forecasting.

Data availability statement

The original contribution presented in the study are included in the article/[supplementary material](#), further inquiries can be directed to the corresponding author.

Author contributions

The authors confirm contribution to the paper as follows: OD: Data collection, analysis and interpretation of results, data visualization and figures, draft manuscript preparation, review of the final manuscript. JW: Study conception, design and supervision, interpretation of results, draft manuscript preparation, review of the final manuscript. FR: Interpretation of results, review of the final manuscript. JM: Review of the final manuscript. All authors approved the final version of the manuscript.

References

- Ably, G. J., Carroll, M. R., Palmer, M. R., Martí, J., and Sparks, R. S. J. (1998). Basanite-phonolite lineages of the teide-pico Viejo volcanic complex, Tenerife, canary islands. *J. Petrology* 39, 905–936. doi:10.1093/ptro/39.5.905
- Ably, G. J., Ernst, G., Martí, J., and Sparks, R. S. J. (1995). The ~2 ka subplinian eruption of Montaña Blanca. *Tenerife. Bull. Volcanol.* 57, 337–355. doi:10.1007/BF00301292
- Ably, G. J. (1997). *Evolution of the teide-pico Viejo volcanic complex and magmatic system (Tenerife, canary islands)*.
- Ably, G. J., and Martí, J. (2000). Stratigraphy, structure, and volcanic evolution of the Pico teide-pico Viejo formation, Tenerife, canary islands. *J. Volcanol. Geotherm. Res.* 103, 175–208. doi:10.1016/S0377-0273(00)00224-9
- Aigner-Torres, M., Blundy, J., Ulmer, P., and Petteke, T. (2007). Laser Ablation ICPMS study of trace element partitioning between plagioclase and basaltic melts: An experimental approach. *Contributions Mineralogy Petrology* 153, 647–667. doi:10.1007/s00410-006-0168-2
- Albert, H., Costa, F., and Martí, J. (2015a). Timing of magmatic processes and unrest associated with mafic historical monogenetic eruptions in Tenerife Island. *J. Petrology* 56, 1945–1966. doi:10.1093/ptrology/egv058
- Albert, H., Perugini, D., and Martí, J. (2015b). Fractal analysis of enclaves as a new tool for estimating rheological properties of magmas during mixing: The case of Montaña Reventada (Tenerife, canary islands). *Pure Appl. Geophys* 172, 1803–1814. doi:10.1007/s00024-014-0917-5
- Ancochea, E., Fuster, J., Ibarrola, E., Cendrero, A., Coello, J., Hernan, F., et al. (1990). Volcanic evolution of the island of Tenerife (Canary Islands) in the light of new K-Ar data. *J. Volcanol. Geotherm. Res.* 44, 231–249. doi:10.1016/0377-0273(90)90019-C

Funding

OD and JM have been partially funded by, E.G., grant EVE (DG ECHO H2020 Ref. 826292) and the CSIC grant MAPCAN (CSIC Ref. 202130E083). OD was also supported by the Ministry of Science, Innovation, and Universities of Spain with a FPU grant (FPU18/02572) and a mobility grant (EST19/00297). FR was funded by the New Mexico State University Johnson Mass Spectrometry Laboratory (Las Cruces, New Mexico).

Acknowledgments

We thank the reviewers Dr. Kuritani, Dr. Pang, Dr. Davoudian Dr. Fazlnia, and the editor Hossein Azizi, for their helpful comments that have enhanced the quality of the final work. The help from Adelina Geyer in revising the figures was highly appreciated. We also express our sincere appreciation to Scott Borough, Arron Steiner, and Ashley Steiner for technical assistance.

Conflict of interest

The authors declare that the research was conducted in the absence of any commercial or financial relationships that could be construed as a potential conflict of interest.

Publisher's note

All claims expressed in this article are solely those of the authors and do not necessarily represent those of their affiliated organizations, or those of the publisher, the editors and the reviewers. Any product that may be evaluated in this article, or claim that may be made by its manufacturer, is not guaranteed or endorsed by the publisher.

Supplementary material

The Supplementary Material for this article can be found online at: <https://www.frontiersin.org/articles/10.3389/feart.2023.1155724/full#supplementary-material>

- Araña, V., Barberi, F., and Ferrar, G. (1989). "El complejo volcánico teide-pico Viejo," in *Los volcanes y la Caldera del Parque Nacional del Teide (Tenerife, Islas Canarias)*. Editors V. Araña and J. Coello (Madrid: Publicaciones de Iona, Serie Técnica.), 101–127.
- Araña, V. (1971). Litología y estructura del Edificio Cañadas, Tenerife (Islas Canarias). *Estud. Geol.* 27, 95–135.
- Araña, V., Martí, J., Aparicio, A., García-Cacho, L., and García-García, R. (1994). Magma mixing in alkaline magmas: An example from Tenerife, Canary Islands. *Lithos* 32, 1–19. doi:10.1016/0024-4937(94)90018-3
- Azzilli, F., Fabbriozzi, A., Schmidt, M. W., Petrelli, M., Maimaiti, M., Dingwell, D. B., et al. (2018). The effect of diffusive re-equilibration time on trace element partitioning between alkali feldspar and trachytic melts. *Chem. Geol.* 495, 50–66. doi:10.1016/j.chemgeo.2018.07.035
- Astbury, R. L., Petrelli, M., Ubide, T., Stock, M. J., Arienzo, I., D'Antonio, M., et al. (2018). Tracking plumbing system dynamics at the Campi Flegrei caldera, Italy: High-resolution trace element mapping of the Astroni crystal cargo. *Lithos* 318–319, 464–477. doi:10.1016/J.LITHOS.2018.08.033
- Bachmann, O., and Bergantz, G. W. (2006). Gas percolation in upper-crustal silicic crystal mushes as a mechanism for upward heat advection and rejuvenation of near-solidus magma bodies. *J. Volcanol. Geotherm. Res.* 149, 85–102. doi:10.1016/J.JVOLGEORES.2005.06.002
- Bachmann, O., and Bergantz, G. W. (2008). Rhyolites and their source mushes across tectonic settings. *J. Petrology* 49, 2277–2285. doi:10.1093/PETROLOGY/EGN068
- Bachmann, O., Deering, C. D., Lipman, P. W., and Plummer, C. (2014). Building zoned ignimbrites by recycling silicic cumulates: insight from the 1,000 km³ Carpenter Ridge Tuff, CO. *Contrib. Mineral Petrol* 167, 1025. doi:10.1007/s00410-014-1025-3
- Balcells, R., and Hernández-Pacheco, A. (1989). "El domo-colada de Los roques blancos," in *Los volcanes y la Caldera del Parque Nacional del Teide (Tenerife, Islas Canarias)*. Editors V. Araña and J. Coello (Madrid: Publicaciones de Iona, Serie Técnica.), 227–235.
- Bédard, J. H. (2006). Trace element partitioning in plagioclase feldspar. *Geochim. Cosmochim. Acta* 70, 3717–3742. doi:10.1016/j.gca.2006.05.003
- Bindeman, I. N., Davis, A. M., and Drake, M. J. (1998). Ion microprobe study of plagioclase-basalt partition experiments at natural concentration levels of trace elements. *Geochim. Cosmochim. Acta* 62, 1175–1193. doi:10.1016/s0016-7037(98)00047-7
- Bindeman, I. N., and Davis, A. M. (2000). Trace element partitioning between plagioclase and melt: Investigation of dopant influence on partition behavior. *Geochim. Cosmochim. Acta* 64, 2863–2878. doi:10.1016/s0016-7037(00)00389-6
- Blundy, J. D., and Wood, B. J. (1991). Crystal-chemical controls on the partitioning of Sr and Ba between plagioclase feldspar, silicate melts, and hydrothermal solutions. *Geochimica et Cosmochimica Acta* 55, 193–209. doi:10.1016/0016-7037(91)90411-w
- Blundy, J., and Wood, B. (2003). Partitioning of trace elements between crystals and melts. *Earth Planet Sci. Lett.* 210, 383–397. doi:10.1016/S0012-821X(03)00129-8
- Blundy, J., and Wood, B. (1994). Prediction of crystal–melt partition coefficients from elastic moduli. *Nature* 372, 452–454. doi:10.1038/372452a0
- Brändle, J. L. (1973). Evolución geoquímica de los materiales volcánicos sálicos y alcalinos de la isla de Tenerife. *Estud. Geol.* 29, 5–21.
- Brown, B. S., Ramos, F. C., Wolff, J. A., Dorado, O., and Martí, J. (2022). Unleashing alkali feldspar: Ra/Th ages and chemical and isotopic constraints on Holocene phonolite magmatism, canary islands. *Geology* 50, 1106–1110. doi:10.1130/G50112.1
- Brown, R. J., Barry, T. L., Branney, M. J., Pringle, M. S., and Bryan, S. E. (2003). The quaternary pyroclastic succession of southeast Tenerife, canary islands: Explosive eruptions, related caldera subsidence, and sector collapse. *Geol. Mag.* 140, 265–288. doi:10.1017/S0016756802007252
- Browne, B. L., Eichelberger, J. C., Patino, L. C., Vogel, T. A., Uto, K., and Hoshizumi, H. (2006). Magma mingling as indicated by texture and Sr/Ba ratios of plagioclase phenocrysts from Unzen volcano, SW Japan. *J. Volcanol. Geotherm. Res.* 154, 103–116. doi:10.1016/J.JVOLGEORES.2005.09.022
- Cabrera Lagunilla, P., and Hernández Pacheco, A. (1987). in *Las erupciones históricas de Tenerife (Canarias) en sus aspectos vulcanológicos, petrológico y geoquímico* (Madrid: Revista de materiales y procesos geológicos), 143–182, 143–182.
- Carracedo, J. C., Paterne, M., Guillou, H., Perez-Torrado, F. J., Paris, R. M., Rodriguez-Badiola, E., et al. (2003). *Dataciones radiométricas (14C y K/Ar) del Teide y el rift noroeste, Tenerife, Islas Canarias*. Madrid: Estudios Geológicos.
- Carracedo, J. C., Rodríguez Badiola, E., Guillou, H., Paterne, M., Scaillet, S., Pérez Torrado, F. J., et al. (2007). Eruptive and structural history of Teide volcano and rift zones of Tenerife, canary islands. *GSA Bull.* 119, 1027–1051. doi:10.1130/B26087.1
- Cas, R. A. F., Wolff, J. A., Martí, J., Olin, P. H., Edgar, C. J., Pittari, A., et al. (2022). Tenerife, a complex end member of basaltic oceanic island volcanoes, with explosive polygenetic phonolitic calderas, and phonolitic-basaltic stratovolcanoes. *Earth Sci. Rev.* 230, 103990. doi:10.1016/J.EARSCIREV.2022.103990
- Costa, F., Chakraborty, S., and Dohmen, R. (2003). Diffusion coupling between trace and major elements and a model for calculation of magma residence times using plagioclase. *Geochim. Cosmochim. Acta* 67, 2189–2200. doi:10.1016/s0016-7037(02)01345-5
- Couch, S., Sparks, R. S. J., and Carroll, M. R. (2001). Mineral disequilibrium in lavas explained by convective self-mixing in open magma chambers. *Nature* 411, 1037–1039. doi:10.1038/35082540
- Deer, W. A., Howie, R. A., and Zussman, J. (1992). *An introduction to the rock-forming minerals*. London: Mineralogical Society of Great Britain and Ireland. doi:10.1180/dhz
- di Roberto, A., Bertagnini, A., del Carlo, P., Meletlidis, S., and Pompilio, M. (2016). The 1909 chinero eruption on Tenerife (canary islands): Insights from historical accounts, and tephrostratigraphic and geochemical data. *Bull. Volcanol.* 78, 1–17. doi:10.1007/S00445-016-1083-7
- Dohmen, R., and Blundy, J. (2014). A predictive thermodynamic model for element partitioning between plagioclase and melt as a function of pressure, temperature and composition. *Am. J. Sci.* 314, 1319–1372. doi:10.2475/09.2014.04
- Dorado, O., Andújar, J., Martí, J., and Geyer, A. (2021). Pre-eruptive conditions at satellite vent eruptions at teide-pico Viejo complex (Tenerife, canary islands). *Lithos* 396–397, 106193. doi:10.1016/J.LITHOS.2021.106193
- D'Orlando, C., Landi, P., Pimentel, A., and Zanon, V. (2017). Magmatic processes revealed by anorthoclase textures and trace element modeling: The case of the Lajes Ignimbrite eruption (Terceira Island, Azores). *J. Volcanol. Geotherm. Res.* 347, 44–63. doi:10.1016/J.JVOLGEORES.2017.08.012
- Edgar, C. J., Cas, R. A. F., Olin, P. H., Wolff, J. A., Martí, J., and Simmons, J. M. (2017). Causes of complexity in a fallout dominated plinian eruption sequence: 312 ka fasnía member, Diego Hernández Formation, Tenerife, Spain. *J. Volcanol. Geotherm. Res.* 345, 21–45. doi:10.1016/j.jvolgeores.2017.07.008
- Edgar, C. J., Wolff, J. A., Nicholls, H. J., Cas, R. A. F., and Martí, J. (2002). A complex quaternary ignimbrite-forming phonolitic eruption: The poris member of the Diego Hernández Formation (Tenerife, canary islands). *J. Volcanol. Geotherm. Res.* 118, 99–130. doi:10.1016/s0377-0273(02)00252-4
- Edgar, C. J., Wolff, J. A., Olin, P. H., Nichols, H. J., Pittari, A., Cas, R. A. F., et al. (2007). The late Quaternary Diego Hernandez Formation, Tenerife: Volcanology of a complex cycle of voluminous explosive phonolitic eruptions. *J. Volcanol. Geotherm. Res.* 160, 59–85. doi:10.1016/J.JVOLGEORES.2006.06.001
- Fabbriozzi, A., Schmidt, M. W., Günther, D., and Eikenberg, J. (2009). Experimental determination of Ra mineral/melt partitioning for feldspars and 226Ra-disequilibrium crystallization ages of plagioclase and alkali-feldspar. *Earth Planet Sci. Lett.* 280, 137–148. doi:10.1016/j.epsl.2009.01.022
- Fernández Satín, S., and Vicente-Mingarro, I. (1989). Geochemical study of the historic eruptions of the Canary Islands. *Rev. Mat. Procesos Geol.* 6, 99–155.
- Foley, M. L., Miller, C. F., and Gualda, G. A. R. (2020). Architecture of a super-sized magma chamber and remobilization of its basal cumulate (peach spring tuff, USA). *J. Petrology* 61, 20. doi:10.1093/PETROLOGY/EGAA020
- Fuster, J. M., Araña, V., Brande, J. L., Navarro, J. M., Alonso, U., and Aparicio, A. (1968). *Geología y vulcanología de las islas Canarias: Tenerife, ed. I*. Madrid: Lucas Mallada" CSIC.
- García Moral, R. (1989). "Erupciones históricas en Tenerife," in *Los volcanes y la Caldera del Parque Nacional del Teide (Tenerife, Islas Canarias)*. Editors V. Araña and J. Coello (Madrid: Publicaciones de Iona, Serie Técnica.), 235–252.
- García, O., Bonadonna, C., Martí, J., and Pioli, L. (2012). The 5,660 yBP boquerón explosive eruption, teide-pico Viejo complex, Tenerife. *Bull. Volcanol.* 74, 2037–2050. doi:10.1007/s00445-012-0646-5
- Giacomoni, P. P., Ferlito, C., Coltorti, M., Bonadiman, C., and Lanzafame, G. (2014). Plagioclase as archive of magma ascent dynamics on "open conduit" volcanoes: The 2001–2006 eruptive period at Mt. Etna. *Earth Sci. Rev.* 138, 371–393. doi:10.1016/j.earscirev.2014.06.009
- González-García, D., Petrelli, M., Perugini, D., Giordano, D., Vasseur, J., Paredes-Mariño, J., et al. (2022). Pre-eruptive conditions and dynamics recorded in banded pumices from the El Abrigo caldera-forming eruption (Tenerife, canary islands). *J. Petrology* 63, 1–24. doi:10.1093/PETROLOGY/EGAC009
- Guillou, H., Carracedo, J. C., Paris, R., and Torrado, F. J. P. (2004). Implications for the early shield-stage evolution of Tenerife from K/Ar ages and magnetic stratigraphy. *Earth Planet Sci. Lett.* 222, 599–614. doi:10.1016/J.EPSL.2004.03.012
- Guillou, H., Kissel, C., Laj, C., and Carracedo, J. C. (2013). Dating the Teide volcanic complex: Radiometric and palaeomagnetic methods. *Act. Volcanoes World*, 93–103. doi:10.1007/978-3-642-25893-0_6/FIGURES/9
- Henderson, C. M. B., and Pierozynski, W. J. (2012). An experimental study of Sr, Ba and Rb partitioning between alkali feldspar and silicate liquid in the system nepheline-kalsilite-quartz at 0.1 GPa P (H 2 O): A revisitiation and reassessment. *Mineral. Mag.* 76, 157–190. doi:10.1180/minmag.2012.076.1.157
- Hildreth, W. (2004). Volcanological perspectives on long valley, mammoth mountain, and mono craters: Several contiguous but discrete systems. *J. Volcanol. Geotherm. Res.* 136, 169–198. doi:10.1016/j.jvolgeores.2004.05.019

- Huber, C., Bachmann, O., and Dufek, J. (2012). Crystal-poor versus crystal-rich ignimbrites: A competition between stirring and reactivation. *Geology* 40, 115–118. doi:10.1130/G32425.1
- Huber, C., Bachmann, O., and Manga, M. (2009). Homogenization processes in silicic magma chambers by stirring and mushification (latent heat buffering). *Earth Planet Sci. Lett.* 283, 38–47. doi:10.1016/j.epsl.2009.03.029
- Humphreys, M. C. S., Blundy, J. D., and Sparks, R. S. J. (2006). Magma evolution and open-system processes at shiveluch volcano: Insights from phenocryst zoning. *J. Petrology* 47, 2303–2334. doi:10.1093/PETROLOGY/EGL045
- Hunt, J. E., Cassidy, M., and Talling, P. J. (2018). Multi-stage volcanic island flank collapses with coeval explosive caldera-forming eruptions. *Sci. Rep.* 8, 1146. doi:10.1038/s41598-018-19285-2
- Ibarrola, M. E. (1970). Variability of basaltic magmas in the eastern and central Canary Islands. *Estud. Geol.* 26, 337–399.
- Icenhower, J., and London, D. (1996). Experimental partitioning of Rb, Cs, Sr, and Ba between alkali feldspar and peraluminous melt. *Am. Mineralogist* 81 (5–6), 719–734. doi:10.2138/am-1996-5-619
- Kent, A. J. R., Darr, C., Koleszar, A. M., Salisbury, M. J., and Cooper, K. M. (2010). Preferential eruption of andesitic magmas through recharge filtering. *Nat. Geosci.* 3 (9), 631–636. doi:10.1038/ngeo924
- Landi, P., la Felice, S., Petrelli, M., Vezzoli, L. M., and Principe, C. (2019). Deciphering textural and chemical zoning of K-feldspar megacrysts from Mt. Amiata Volcano (Southern Tuscany, Italy): Insights into the petrogenesis and abnormal crystal growth. *Lithos* 2019, 569–583. doi:10.1016/J.LITHOS.2018.11.032
- Le Bas, M. J., Maitre, L., and Zanettin, B. (1986). A Chemical Classification of Volcanic Rocks Based on the Total Alkali-Silica Diagram. *J. Petrology* 27(3), 745–750.
- Long, P. E. (1978). Experimental determination of partition coefficients for Rb, Sr and Ba between alkali feldspar and silicate liquid. *Geochim. Cosmochim. Acta* 42, 833–846. doi:10.1016/0016-7037(78)90096-0
- Martí, J., Geyer, A., Andujar, J., Teixidó, F., and Costa, F. (2008). Assessing the potential for future explosive activity from teide-pico Viejo stratovolcanoes (Tenerife, canary islands). *J. Volcanol. Geotherm. Res.* 178, 529–542. doi:10.1016/J.JVOLGEORES.2008.07.011
- Martí, J., and Gudmundsson, A. (2000). The las Cañadas caldera (Tenerife, canary islands): An overlapping collapse caldera generated by magma-chamber migration. *J. Volcanol. Geotherm. Res.* 103, 161–173. doi:10.1016/S0377-0273(00)00221-3
- Martí, J., Hurlimann, M., Ablay, G. J., and Gudmundsson, A. (1997). Vertical and lateral collapses on Tenerife (Canary Islands) and other volcanic ocean islands. *Geology* 25 (10), 879–882. doi:10.1130/0091-7613(1997)025<0879:valcot>2.3.co;2
- Martí, J., Mitjavila, J., and Araña, V. (1994). Stratigraphy, structure and geochronology of the las Cañadas caldera (Tenerife, canary islands). *Geol. Mag.* 131, 715–727. doi:10.1017/S0016756800012838
- Martí, J., Zafrilla, S., Andujar, J., Jiménez-Mejías, M., Scaillet, B., Pedrazzi, D., et al. (2020). Controls of magma chamber zonation on eruption dynamics and deposits stratigraphy: The case of El Palomar fallout succession (Tenerife, Canary Islands). *J. Volcanol. Geotherm. Res.* 399, 106908. doi:10.1016/j.jvolgeores.2020.106908
- Neumann, E., Wulff-Pedersen, E., Simonsen, S., Pearson, N., Martí, J., and Mitjavila, J. (1999). Evidence for fractional crystallization of periodically refilled magma chambers in Tenerife. *Canary Isl.* 1999. doi:10.1093/PETROJ/40.7.1089
- Onuma, N., Higuchi, H., Wakita, H., and Nagasawa, H. (1968). Trace element partition between two pyroxenes and the host lava. *Earth Planet Sci. Lett.* 5, 47–51. doi:10.1016/S0012-821X(68)80010-X
- Ovchinnikova, G. v., Belyatskii, B. v., Vasil'eva, I. M., Levskii, L. K., Grachev, A. F., Araña, V., et al. (1995). Sr–Nd–Pb isotope characteristics of the mantle sources of basalts from the Canary Islands. *Petrology* 3, 172–182.
- Pittari, A. (2004). *Eruption dynamics and emplacement processes for the climactic Abrigo Member*. Tenerife, Canary Islands: Doctoral dissertation, Monash University.
- Ramos, F. C., and Tepley, F. J. (2008). Inter- and intracrystalline isotopic disequilibria: Techniques and applications. *Rev. Mineral. Geochem* 69, 403–443. doi:10.2138/RMG.2008.69.11
- Ramos, F. C., Wolff, J. A., Buettner, J. E., Wei, H. Q., and Xu, J. (2019). Ra/Th ages of sanidine in young trachytes erupted at Changbaishan Volcano, China. *J. Volcanol. Geotherm. Res.* 374, 226–241. doi:10.1016/j.jvolgeores.2019.02.006
- Ridley, W. I. (1970). The Petrology of the las canadas volcanoes, Tenerife, canary islands. *Contr. Mineral. Pet.* 26, 124–160. doi:10.1007/bf00371260
- Risica, G., di Roberto, A., Speranza, F., del Carlo, P., Pompilio, M., Meletlidis, S., et al. (2020). Refining the Holocene eruptive activity at Tenerife (canary islands): The contribution of palaeomagnetism. *J. Volcanol. Geotherm. Res.* 401, 106930. doi:10.1016/j.jvolgeores.2020.106930
- Rodríguez Badiola, E., Pérez Torrado, F. J., Carracedo, J. C., and Guillou, H. (2006). “Petrografía y geoquímica del edificio volcánico Teide-Pico Viejo y las dorsales noreste y noroeste de Tenerife,” in *Los volcanes del Parque Nacional del Teide* (Madrid: Organismo Autónomo Parques Nacionales, Ministerio de Medio Ambiente), 129–188.
- Salisbury, M. J., Bohrer, W. A., Clynne, M. A., Ramos, F. C., and Hoskin, P. (2008). Multiple plagioclase crystal populations identified by crystal size distribution and *in situ* chemical data: Implications for timescales of magma chamber processes associated with the 1915 eruption of lassen peak, CA. *J. Petrology* 49, 1755–1780. doi:10.1093/PETROLOGY/EGN045
- Schoneveld, L., and O'Neill, H. S. C. (2019). The influence of melt composition on the partitioning of trace elements between anorthite and silicate melt. *Contributions Mineralogy Petrology* 174, 13. doi:10.1007/s00410-019-1548-8
- Sliwinski, J. T., Bachmann, O., Ellis, B. S., Dávila-Harris, P., Nelson, B. K., and Dufek, J. (2015). Eruption of shallow crystal cumulates during explosive phonolitic eruptions on Tenerife, Canary Islands. *J. Petrology* 56, 2173–2194. doi:10.1093/petrology/egv068
- Sparks, R. S. J., Annen, C., Blundy, J. D., Cashman, K. v., Rust, A. C., and Jackson, M. D. (2019). Formation and dynamics of magma reservoirs. *Philosophical Trans. R. Soc. A Math. Phys. Eng. Sci.* 377, 20180019. doi:10.1098/rsta.2018.0019
- Sun, S. S., and McDonough, W. F. (1989). Chemical and isotopic systematics of oceanic basalts: Implications for mantle composition and processes. *Geol. Soc. Spec. Publ.* 42, 313–345. doi:10.1144/GSL.SP.1989.042.01.19
- Sundermeyer, C., Gätjen, J., Weimann, L., and Wörner, G. (2020). Timescales from magma mixing to eruption in alkaline volcanism in the Eifel volcanic fields, Western Germany. *Contributions Mineralogy Petrology* 175, 77–23. doi:10.1007/s00410-020-01715-y
- Tepley, F. J., Lundstrom, C. C., McDonough, W. F., and Thompson, A. (2010). Trace element partitioning between high-An plagioclase and basaltic to basaltic andesite melt at 1 atmosphere pressure. *Lithos* 118, 82–94. doi:10.1016/j.lithos.2010.04.001
- Thirlwall, M. F., Singer, B. S., and Marriner, G. F. (2000). 39Ar-40Ar ages and geochemistry of the basaltic shieldstage of Tenerife, Canary Islands, Spain. *J. Volcanol. Geotherm. Res.* 103, 247–297. doi:10.1016/S0377-0273(00)00227-4
- Triebeold, S., Kronz, A., and Wörner, G. (2006). Anorthite-calibrated backscattered electron profiles, trace elements, and growth textures in feldspars from the Teide–Pico Viejo volcanic complex (Tenerife). *J. Volcanol. Geotherm. Res.* 154, 117–130. doi:10.1016/J.JVOLGEORES.2005.09.023
- Watts, A. B., Peirce, C., Collier, J., Dalwood, R., Canales, J. P., and Henstock, T. J. (1997). A seismic study of lithospheric flexure in the vicinity of Tenerife, Canary Islands. *Earth Planet Sci. Lett.* 146, 431–447. doi:10.1016/S0012-821X(96)00249-x
- Whitney, D. L., and Evans, B. W. (2010). Abbreviations for names of rock-forming minerals. *Am. mineralogist* 95, 185–187. doi:10.2138/am.2010.3371
- Wiesmaier, S., Deegan, F. M., Troll, V. R., Carracedo, J. C., Chadwick, J. P., and Chew, D. M. (2011). Magma mixing in the 1100 AD Montaña Reventada composite lava flow, Tenerife, Canary Islands: Interaction between rift zone and central volcano plumbing systems. *Contributions Mineralogy Petrology* 162, 651–669. doi:10.1007/S00410-010-0596-X
- Wolff, J. A., Ellis, B. S., Ramos, F. C., Starkel, W. A., Boroughs, S., Olin, P. H., et al. (2015). Remelting of cumulates as a process for producing chemical zoning in silicic tuffs: A comparison of cool, wet and hot, dry rhyolitic magma systems. *Lithos* 236–237, 275–286. doi:10.1016/J.LITHOS.2015.09.002
- Wolff, J. A., Forni, F., Ellis, B. S., and Szymanowski, D. (2020). Europium and barium enrichments in compositionally zoned felsic tuffs: A smoking gun for the origin of chemical and physical gradients by cumulate melting. *Earth Planet Sci. Lett.* 540, 116251. doi:10.1016/J.EPSL.2020.116251
- Wolff, J. A. (2017). On the syenite-trachyte problem. *Geology* 45, 1067–1070. doi:10.1130/G39415.1